UNIVERSITÀ DEGLI STUDI DI NAPOLI
"FEDERICO II"

Scuola Politecnica e delle Scienze di Base

Area Didattica di Scienze Matematiche Fisiche e Naturali

Dipartimento di Fisica "Ettore Pancini"

Laurea Magistrale in Fisica

The transplanckian problem for initial conditions of perturbations during inflation: a stochastic model and a likelihood analysis of parameters

Relatori:
Prof. Gianpiero Mangano
Dott. Mattia Cielo

Candidato:
Lorenzo Cirillo
Matr. N94000701

Anno Accademico 2023/2024

A mia madre
e Giovanni

CONTENTS

Introduction **iv**

1 Standard Cosmology **1**

1.1 Cosmological scales . . . 3

1.1.1 Curvature Radius of the Universe . . . 3

1.1.2 Hubble Radius . . . 4

1.1.3 Particle Horizon . . . 4

1.2 The shortcomings of the Standard Cosmological Model . . . 5

1.2.1 The flatness problem . . . 5

1.2.2 The horizon problem . . . 6

1.2.3 Fluctuation correlations . . . 8

2 Inflation: the background **11**

2.1 Standard inflationary dynamics . . . 11

2.2 General constraints . . . 12

2.2.1 Duration of inflation . . . 12

2.2.2 SEC violation and quasi-de Sitter stage . . . 13

2.3 Scalar field model . . . 14

2.3.1 Slow-roll conditions . . . 15

2.3.2 Chaotic inflationary potential . . . 17

2.4 Reheating . . . 18

3 Inflation: Perturbations **21**
3.1 Linear perturbations . . . 22
3.1.1 Metric perturbations . . . 22
3.1.2 Matter perturbations . . . 25
3.1.3 Conservation and Einstein equations . . . 27
3.2 Quantum initial conditions . . . 29
3.2.1 Classical equations . . . 29
3.2.2 Classical solutions . . . 32
3.2.3 Quantum fluctuations . . . 33
3.2.4 Evidences and open problems . . . 37
3.2.5 The trans-Planckian problem . . . 38

4 Initial conditions: a stochastic model **40**
4.1 Limits of the perturbation theory . . . 40
4.2 Tensor perturbation evolution . . . 41
4.3 The shear source model . . . 43
4.4 Results . . . 43
4.5 Outlooks . . . 44
4.6 The main idea . . . 45

5 Bayesian Methods **46**
5.1 Basic Notions . . . 46
5.2 Inference and likelihood . . . 47
5.3 Bayesian inference . . . 48
5.3.1 Bayes theorem . . . 48
5.3.2 Choice of the prior . . . 49
5.3.3 Model selection . . . 50
5.4 Numerical applications . . . 51
5.4.1 Markov chain Monte Carlo (MCMC) . . . 51
5.4.2 Nested sampling . . . 52
5.5 The codes . . . 54
5.5.1 CAMB . . . 54
5.5.2 Cobaya . . . 55

6 Stochastic model parameter analysis **61**
6.1 Preliminary amplitude decomposition . . . 62
6.2 Analysis of Λ . . . 63

Conclusions **73**

Bibliography **75**

INTRODUCTION

Cosmic inflation is a theory within the field of cosmology that proposes a rapid and exponential expansion of the universe during the earliest moments of its existence. This period of inflation is believed to have occurred just fractions of a second after the Big Bang, leading to the vast and homogeneous cosmos we observe today.

The idea of cosmic inflation was first proposed in the early 1980s to address several outstanding problems in the standard Big Bang model of cosmology. One of the key issues it seeks to resolve is known as the horizon problem. This problem arises from the observation that distant regions of the universe, which are separated by vast distances, exhibit remarkably similar properties. According to the standard model, these regions should not have had enough time to interact and reach thermal equilibrium, yet they appear to have the same temperature and density. Cosmic inflation provides a solution to this problem by postulating a period of rapid expansion that would have rendered the entire observable universe causally connected, allowing for thermal equilibrium to be established before the onset of inflation.

In addition to addressing the horizon problem, cosmic inflation offers solutions to other cosmological puzzles, such as the flatness problem and the origin of structure in the universe. The flatness problem refers to the observation that the universe appears to be geometrically flat on large scales, which is unexpected given the dynamics of the expanding universe. Inflationary theory predicts that the universe would have been driven towards flatness during the inflationary epoch, providing a natural explanation for this observed flatness.

Furthermore, cosmic inflation provides a mechanism for the generation of primordial density fluctuations, which are thought to be the seeds of large-scale structure formation in the universe. Quantum fluctuations during the inflationary period are stretched to cosmological scales, leaving imprints in the cosmic microwave background radiation and leading to the formation of galaxies and galaxy clusters.

In summary, cosmic inflation plays a central role in the standard cosmological model by providing solutions to fundamental problems and offering a mechanism for the origin of large-scale structure in the universe. Its theoretical predictions are supported by a wealth of observational evidence, making it a cornerstone of modern cosmology.

CHAPTER

1

STANDARD COSMOLOGY

The universe exhibits a remarkable degree of homogeneity on large scales [9], meaning that its properties appear to be uniform when observed over vast distances. However, this uniformity is not absolute, as evidenced by small-scale anisotropies observed in the cosmic microwave background (CMB) radiation, which provide valuable insights into the early universe. Additionally, the distribution of matter throughout the cosmos is not perfectly uniform, with regions of higher and lower density giving rise to structures such as galaxies, galaxy clusters, and cosmic voids.

Despite these small-scale variations, the universe adheres to the cosmological principle, which posits isotropy and homogeneity on sufficiently large scales. This principle serves as the foundation of the Friedmann-Robertson-Walker (FRW) metric, which describes the large-scale dynamics of the expanding universe. By assuming homogeneity and isotropy on cosmological scales, the FRW metric provides a framework for understanding the overall structure and evolution of the universe.

In this context, it is natural to attribute the small inhomogeneities observed in the distribution of matter and radiation to small deviations of the metric from the homogeneous background metric. From this point on, the background metric will be denoted as:

$$\begin{aligned} ds^2 &= g_{\mu\nu} dx^\mu dx^\nu = \\ &= -dt^2 + a^2(t)\left[\frac{dr^2}{1-kr^2} + r^2 d\theta^2 + r^2 \sin^2\theta d\phi^2\right] \end{aligned} \tag{1.1}$$

where (t, r, θ, ϕ) are comoving coordinates, $a(t)$ is the scale factor and k is a constant, strictly related to the curvature of the universe. The dynamics of the universe in entirely enclosed in the scale factor $a(t)$, whose time dependence is found by inserting it into the Einstein equations

$$G_{\mu\nu} \stackrel{\text{def}}{=} R_{\mu\nu} - \frac{1}{2} g_{\mu\nu} R = 8\pi G\, T_{\mu\nu} - \Lambda g_{\mu\nu} \tag{1.2}$$

together with the conservation laws associated with the energy-momentum tensor

$$\nabla_\mu T^{\mu\nu} = 0 \tag{1.3}$$

In order to comply with the symmetry proprieties of the metric, the stress-energy tensor must also be diagonal. The most effective realization of such a stress-energy tensor is that of a perfect fluid, characterized by a time-dependent energy density $\rho(t)$ and pressure $P(t)$:

$$T^\mu_\nu = \mathrm{diag}\left(-\rho, P, P, P\right) \tag{1.4}$$

As a result of this operation the **Friedmann equations** are obtained:

$$H^2 + \frac{k}{a^2} = \frac{8\pi G}{3}\rho + \frac{\Lambda}{3} \tag{1.5}$$

$$\frac{\ddot{a}}{a} = -\frac{4\pi G}{3}\left(\rho + 3P\right) + \frac{\Lambda}{3} \tag{1.6}$$

with the conservation law

$$\dot{\rho} + 3H\left(\rho + P\right) = 0 \tag{1.7}$$

where $H = \dot{a}/a$ is the **Hubble parameter**.

It is necessary to supplement this set of equations with an equation of state. It is normally assumed that all the matter contained in the universe complies with a linear relationship

$$P = \omega\rho \tag{1.8}$$

This arises from the most known types of fluid: non-relativistic fluids have $\omega_{\rm NR} = 0$, while relativistic matter have $\omega_{\rm R} = 1/3$.

The general solution of the continuity equation 1.7 for a fluid with equation of state 1.8 is

$$\rho a^{3(1+\omega)} = \text{constant} \tag{1.9}$$

which, in terms of the previous cases, results in

$$\begin{aligned} \rho_{\rm NR} a^3 &= \text{constant} \\ \rho_{\rm R} a^4 &= \text{constant} \end{aligned} \tag{1.10}$$

The particular case of $\omega_\Lambda = -1$ corresponds to a constant energy density, called **vacuum energy**:

$$\rho_\Lambda = \text{constant} \tag{1.11}$$

It is useful to recast the Friedmann equation 1.5 as

$$\Omega - 1 = \frac{k}{a^2 H^2} \tag{1.12}$$

where

$$\Omega = \frac{\rho}{\rho_c} \qquad \rho_c = \frac{3H^2}{8\pi G} \text{ (critical density)}$$

Since $a^2H^2 > 0$, there is a correspondence between k and $\Omega - 1$:

$$\begin{aligned} k = +1 \quad &\Longrightarrow \quad \Omega > 1 \quad \text{CLOSED} \\ k = 0 \quad &\Longrightarrow \quad \Omega = 1 \quad \text{FLAT} \\ k = -1 \quad &\Longrightarrow \quad \Omega < 1 \quad \text{OPEN} \end{aligned}$$

1.1 Cosmological scales

In cosmology, various scales are used to describe the size and properties of the universe. Three important scales are the curvature radius of the universe, the Hubble radius, and the particle horizon. For the rest of this paper, the subscript “0” under a cosmological parameter refers to the value of that parameter measured in the present days (e.g. H_0 is the Hubble parameter today).

1.1.1 Curvature Radius of the Universe

The curvature radius of the universe refers to the radius of curvature of the spatial sections of the universe. In a homogeneous and isotropic universe described by the Friedmann-Lemaître-Robertson-Walker (FLRW) metric, the spatial geometry can be open, flat, or closed, depending on the curvature parameter, Ω_k. The curvature radius, denoted as R_{curv}, is related to the curvature parameter as follows:

$$R_{\text{curv}} = \frac{H^{-1}}{\sqrt{|\Omega_k|}} = \frac{H^{-1}}{|\Omega - 1|^{1/2}} \tag{1.13}$$

where Ω_k represents the curvature density parameter.

1.1.2 Hubble Radius

The Hubble radius, denoted as R_{H}, is a measure of the distance at which the recession velocity of objects due to the expansion of the universe equals the speed of light. Mathematically, it is defined as the inverse of the Hubble parameter:

$$R_{\text{H}} = \frac{1}{H} \tag{1.14}$$

Objects beyond the Hubble radius are receding from us faster than the speed of light and are therefore beyond our observable universe. Two particle separated by a distance larger than the Hubble radius at a certain moment of time cannot be causally connected at that instant.

1.1.3 Particle Horizon

The particle horizon represents the maximum distance from which light or any other form of radiation could have reached us since the beginning of the universe. It is determined by the finite age of the universe and the speed of light:

$$d_{\text{H}}(t) = a(t) \int_0^t \frac{dt'}{a(t')} \tag{1.15}$$

As time progresses, the particle horizon increases, allowing us to observe more of the universe. Two particles separated by a distance larger than d_{H} have never been able to communicate since the origin of the universe.

To conclude this section, it is rather important to highlight some aspects of these scales:

- When $|\Omega_k| \ll 1$ the curvature radius turns out to be much larger than the Hubble radius and it is possible to safely neglect the effect of curvature in the universe;
- If R_{H} is finite, it sets the boundary between the visible universe and the part of the universe from which light signals couldn't have reached us;
- In Standard Cosmology the distance to the horizon is finite, and up to numerical factors, equal to the Hubble radius, H^{-1}, but during inflation, they are drastically different.

1.2 The shortcomings of the Standard Cosmological Model

Most issues related to the Standard Cosmological Model concern the quest for initial conditions to be imposed on the equations governing the evolution of the universe, aiming to provide a coherent description of the universe as observed today. Naturally, the search tends to derive assumptions and conditions for the primordial universe that are both simple and general. As will be seen in the following sections, the SCM fails to lead to such conditions or derive general information about the primordial universe.

1.2.1 The flatness problem

In the Standard Cosmological Model, one of the key challenges is known as the flatness problem. This problem arises from the observation that the universe appears to be geometrically flat on large scales, which is unexpected given the dynamics of the expanding universe. Particularly, the issue emerges from the fine-tuning required for the universe to have Ω very close to 1 at early times. Even a small deviation from $\Omega = 1$ in the early universe would lead to a significantly different fate for the universe at late times.

Mathematically, the evolution of the density parameter Ω with time is given by the Friedmann equation 1.12:

$$\Omega_k(t) \propto \frac{\Omega_{k,0}}{H^2 a^2} \tag{1.16}$$

During the MD period of the universe, since the matter-radiation equality, we have $H^2 \propto \rho_{\mathrm{R}} \propto a^{-3}$. Consequently

$$\Omega_k(t_{\mathrm{eq}}) \propto \Omega_{k,0}\, a_{\mathrm{eq}} \tag{1.17}$$

At earlier times, the universe was dominated by radiation, so $H^2 \propto \rho_{\mathrm{R}} \propto a^{-4}$, then

$$\Omega_k(t) \propto \Omega_k(t_{\mathrm{eq}})\, a^2(t) \propto \Omega_{k,0}\, a^2(t) \tag{1.18}$$

As mentioned before, we know from CMB observation that $|\Omega_{k,0}| < 0.005$ [2]. Evaluating the curvature density parameter at the the time of BBN ($z_{\mathrm{BBN}} \simeq 4 \times 10^8$), the result is

$$\Omega_k(t_{\mathrm{BBN}}) < 10^{-16}$$

At even earlier times, the curvature parameter is constrained to be even smaller.

In addition to that, it is possible to correlate the curvature of a region in space with the sum of the potential and kinetic energies of the fluid in that region. Thus, the problem of specifying the initial value for the curvature parameter is strictly related to the task of assigning an initial velocity to the fluid in every point in space. For this reason the flatness problem is often referred as the initial velocities problem. Going back to the Planckian epoch, an error in the initial velocities exceeding $10^{-54}\%$ [9] has a dramatic consequence: the universe either recollapses or becomes "empty" too early.

The fine-tuning of the initial velocities is made even more dramatic by considering it in combination with the horizon problem, which will be discussed in the next section, since the fluid velocities need to be fine-tuned across causally-disconnected regions of space.

1.2.2 The horizon problem

The horizon problem arises from the observation that widely separated regions of the universe have nearly identical properties, despite the fact that they have not had sufficient time to interact or exchange information since the beginning of the universe. This poses a challenge to the understanding of how these regions came to possess similar characteristics.

One of the most effective ways to visualize this mechanism is through the comparison of the horizon scale between the present days and the last-scattering surface. The region of space where matter and radiation are homogeneous and isotropic is at least as large as the present horizon scale

$\lambda_0(t_0) \equiv d_{\rm H}(t_0)$ (which corresponds to the present Hubble radius $R_{\rm H}(t_0)$). The corresponding scale at the time of the last-scattering was smaller by the ratio of the corresponding scale factors:

$$\lambda_0(t_{\rm ls}) = R_{\rm H}(t_0)\left(\frac{a_{\rm ls}}{a_0}\right) = R_H(t_0)\left(\frac{T_0}{T_{\rm ls}}\right) \tag{1.19}$$

On the other hand, during the MD period, the Hubble length has decreased with a different law

$$H^2 \propto \rho_{\rm NR} \propto a^{-3} \propto T^3$$

thus resulting in a radius

$$R_H(t_{\rm ls}) = H^{-1}(t_{\rm ls}) = R_H(t_0)\left(\frac{T_0}{T_{\rm ls}}\right)^{3/2} \ll R_H(t_0) \tag{1.20}$$

The length corresponding to our present Hubble radius is much larger than the causality radius at last-scattering. This can be shown comparing the volumes corresponding to these two scales

$$\frac{\lambda_0^3(t_{\rm ls})}{R_H^3(t_{\rm ls})} = \frac{\lambda_0^3(t_{\rm ls})}{H^{-3}(t_{\rm ls})} = \left(\frac{T_0}{T_{\rm ls}}\right)^{-3/2} \simeq 10^6 \tag{1.21}$$

There were roughly 10^6 causally disconnected regions within the volume that now corresponds to our horizon. This means that the energy density was finely distributed with a fractional variation not exceeding $10^{-2}\%$, despite the fact that particles had never been able to interact with each other since the origin of the universe.

Figure 1.1 shows a useful illustration of the horizon problem.

The above considerations clearly show that the initial conditions which led to the observed universe are very unnatural and non-generic. It seems quite unreasonable and forced to accept that the realization of such a precise and uniform energy distribution is not the result of a single causal physical process. One could imagine that among the various assumptions that can be made about the initial conditions, that of the perfect homogeneity and flatness of the universe is the most symmetric and natural, suitable to be postulated for a theory about the origin of the universe. However, this consideration encounters strong challenges when considering the observed correlation between the fluctuations present in causally disconnected regions of space.

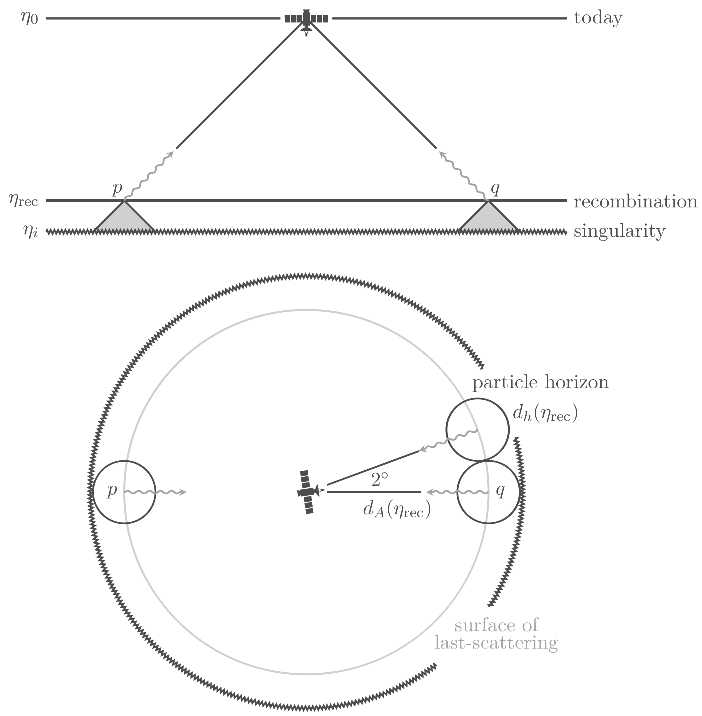

Figure 1.1: *Illustration of the horizon problem in the conventional cosmologycal model taken from ref. [2]. Past light-cones of two points separated by more than 2° do not overlap.*

1.2.3 Fluctuation correlations

Before getting into the specifics of inflation, it is important to describe an additional problem of the SCM.

Fluctuations around the homogeneous and isotropic background not only exist, but appear to be correlated to each other across different regions of space. This poses an additional puzzle to the question of initial conditions. If complete homogeneity is assumed as primordial state of the universe, how could such fluctuations have arisen?

To delve deeper into this topic, it is very helpful to introduce the **conformal time** defined as

$$d\eta = \frac{dt}{a} \tag{1.22}$$

With this definition, it is possible to rewrite the FRW metric as

$$ds^2 = a^2(\eta)\left[-d\eta^2 + d\mathbf{x}^2\right] \tag{1.23}$$

and the comoving particle horizon $d_{\rm H}/a$ as

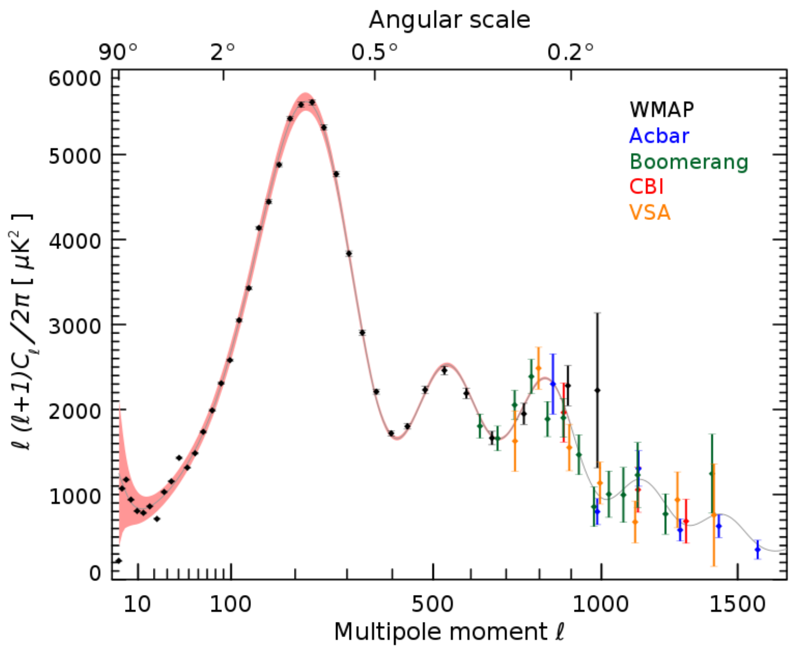

Figure 1.2: *CMB anisotropy as function of multipole moment l, as result of several observations.*

$$d_{\mathrm{H}}(\eta)/a = \int_0^t \frac{dt'}{a(t')} = \int_0^\eta d\eta' = \eta \tag{1.24}$$

Note

From now on the derivative with respect to conformal time will be denoted with a prime

$$f'(\eta) \equiv \frac{df}{d\eta} = a\dot{f}(t) \qquad \mathcal{H} \equiv \frac{a'}{a}$$

It is now possible to calculate the comoving distance between the present time and the last-scattering surface:

$$d_0(\eta_{\mathrm{ls}}) = \int_{\eta_0}^{\eta_{\mathrm{ls}}} d\eta' = \eta_0 - \eta_{\mathrm{ls}} \tag{1.25}$$

The angle subtended today by the horizon at recombination is then

$$\theta = \frac{2\eta_{\mathrm{ls}}}{\eta_0 - \eta_{\mathrm{ls}}} \simeq 2\frac{\eta_{\mathrm{ls}}}{\eta_0} \simeq 2\left(\frac{T_0}{T_{\mathrm{ls}}}\right)^{1/2} \sim 2^\circ \tag{1.26}$$

This shows that two photons separated by an angle greater than 2 degrees were not in causal contact when they were emitted. For this reason, no correlation should be measured between fluctuations above this separation angle. Expanding the two point correlation function in spherical harmonics, this means that no correlations should be observed for multipole moments $l < 100$. Figure 1.2 shows that small anisotropies are present even at $l \ll 100$, thus proving the existence of super-horizon correlations.

CHAPTER

2

INFLATION: THE BACKGROUND

The previous chapter clearly shows that a common element in all the shortcomings of the conventional cosmology is the growing comoving Hubble radius. It plays a fundamental role in determining the number of causally disconnected regions in space and defines the necessary accuracy of the initial velocities. The insertion of an inflationary stage, in compliance with some constraints that will be discussed in the following paragraphs, intervenes precisely on the dynamic of the Hubble sphere, simultaneously addressing all the problems related to it.

2.1 Standard inflationary dynamics

The definition of the inflation is straightforward: *the inflation is a phase of* ***decreasing Hubble radius*** *in the early universe.*

$$\frac{d}{dt}(aH)^{-1} < 0 \tag{2.1}$$

It will now be important to distinguish clearly between the particle horizon and the Hubble radius, since the inflation mechanism is intended to make the particle horizon much larger than the Hubble radius. In this way, particles that cannot interact at a certain point in time may have interacted early on.

By using $aH = \dot{a}$, it is easy to see that the definition 2.1 is equivalent to the condition

$$\ddot{a} > 0 \tag{2.2}$$

so that the inflation can be equivalently defined as *a stage in the early universe of* ***accelerated expansion***. Constraints on its onset and duration can be posed in order to the horizon and flatness problems to be avoided.

2.2 General constraints

In order to further develop the inflationary cosmology there is the necessity to identify the general features of this stage.

First, inflation should start and end sufficiently early in order not to compromise the successful results of the standard model, such as nucleosynthesis. Furthermore, a smooth transition into the decelerated Friedmann expansion must occur. Finally, the universe has to undergo the so called **reheating** phase, in which particles have to reacquire the heat lost during the rapid expansion.

2.2.1 Duration of inflation

A first estimate about the extent of expansion can be made taking into consideration the requirements on the dynamics of the causality horizon. At the very least, all observed fluctuations must have been inside the particle horizon until a certain time in the early universe. Since the particle horizon depends on the history of the scale factor even before inflation (which is not even well determined at this stage), it is very difficult to calculate. For this reason, the stronger assumption is made that our entire observable universe was inside the Hubble radius at the beginning of inflation.

Denoting with the subscript "i" the time of inflation onset and with the subscript "f" the time of its end, we have:

$$(a_0 H_0)^{-1} < (a_i H_i)^{-1} \tag{2.3}$$

The duration of inflation is often expressed in terms of the **number of e-folds**:

$$N \equiv \ln\left(\frac{a_f}{a_i}\right) \tag{2.4}$$

Making the further simplification that the universe is radiation dominated up to the present epoch, that is $H \propto a^{-2}$

$$H_0^{-1}\frac{a_i}{a_f}\frac{a_f}{a_0} \sim H_0^{-1}e^{-N}\frac{T_0}{T_f} \lesssim H_i^{-1} \tag{2.5}$$

we obtain

$$N \gtrsim \ln\left(\frac{T_0}{H_0}\right) + \ln\left(\frac{H_i}{T_f}\right) \simeq 67 + \ln\left(\frac{H_i}{T_f}\right) \tag{2.6}$$

The conclusion is therefore that in order to address the horizon problem, inflation must last at least 70 Hubble times (e-folds).

2.2.2 SEC violation and quasi-de Sitter stage

Another characteristic of the inflation concerns the type of fluid that dominates the universe during this stage. Directly from the definition of inflation and from Friedmann equation 1.6 it follows that

$$\ddot{a} > 0 \Longleftrightarrow (\rho + 3P) < 0 \tag{2.7}$$

In other words, the fluid that fills the space must violate the so called **Strong Energy Condition**, namely $(\rho + 3P) > 0$. Therefore, an acceleration in the expansion is obtainable only if the pressure of the fluid is negative. Even if counterintuitive, such a kind of fluid has already been encountered in cosmology. Dark energy (cosmological constant) has an equation of state

$$P = -\rho \tag{2.8}$$

The dynamics of a universe dominated by this fluid is time invariant ($H =$ const.) and the metric solution takes the name of *de Sitter* spacetime:

$$ds^2 = -dt^2 + e^{2Ht}d\mathbf{x}^2 \tag{2.9}$$

so that the scale factor grows exponentially. Clearly, this solution does not allow a graceful exit into the radiation dominated phase, so time invariance must be broken, and the Hubble parameter must vary in time. The de Sitter spacetime, however, still remains a good approximation for the inflationary dynamics, which is why inflation is often described as a quasi-de Sitter stage.

Taking the time derivative of the comoving Hubble radius we obtain

$$\frac{d}{dt}(aH)^{-1} = -\frac{\dot{a}H + a\dot{H}}{(aH)^2} = -\frac{1}{a}(1-\varepsilon) \tag{2.10}$$

where ε is the **first slow-roll parameter**, defined as:

$$\varepsilon \equiv -\frac{\dot{H}}{H^2} = -\frac{d(\ln H)}{dN} \tag{2.11}$$

The condition of the shrinking Hubble sphere requires $\varepsilon < 1$. This relation has to be satisfied for the whole duration of the inflation, so the **second slow-roll parameter**[1] is defined specifically to verify this requirement:

$$\eta \equiv \frac{d(\ln \varepsilon)}{dN} = \frac{\dot{\varepsilon}}{H\varepsilon} < 1 \tag{2.12}$$

2.3 Scalar field model

The scalar field has emerged as the leading candidate for realizing the necessary equation of state during the inflationary epoch in cosmology. This preference stems from its versatility and ability to accommodate the key requirements for inflation. Unlike other fields with more complex dynamics, such as vector or tensor fields, scalar fields possess a single degree of freedom, making them more amenable to theoretical analysis and model building. Additionally, scalar fields can exhibit a wide range of behaviors, allowing for the implementation of various inflationary scenarios that can reproduce observed cosmological features. Moreover, scalar fields naturally lend themselves to the generation of the required energy density fluctuations responsible for seeding the large-scale structures observed in the universe today.

Such a scalar field, indicated with $\phi(t, \mathbf{x})$, is called **inflaton**. Associated with each value of the field is a potential energy density $V(\phi)$. The purpose is to find the features of the inflaton necessary to drive inflation. Beginning with the action in a generic spacetime metric:

$$S = \int d^4x\sqrt{-g}\mathcal{L} = \int d^4x\sqrt{-g}\left[-\frac{1}{2}\partial_\mu\phi\partial^\mu\phi - V(\phi)\right] \tag{2.13}$$

[1] Explicit distinction will be made with conformal time if some ambiguity is left by the context.

Using the FRW metric[2] ($\sqrt{-g} = a^3$) and considering the variation $\phi \to \phi + \delta\phi$, the Klein-Gordon equation is obtained:

$$\ddot{\phi} + 3H\dot{\phi} - \frac{\nabla^2\phi}{a^2} + \frac{\partial V}{\partial\phi} = 0 \tag{2.14}$$

The term associated with the expansion rate is called **friction term**, showing that the inflaton encounters a resistance due to the spacetime expansion.

Next, it is important to write the energy-momentum tensor in order to calculate the corresponding energy density and pressure density:

$$T_{\mu\nu} = \partial_\mu\phi\partial_\nu\phi + g_{\mu\nu}\mathcal{L} \tag{2.15}$$

$$\rho = T_{00} = \frac{1}{2}\dot{\phi}^2 + V(\phi) + \frac{(\nabla\phi)^2}{2a^2} \tag{2.16}$$

$$P = \frac{T^i_i}{3} = \frac{1}{2}\dot{\phi}^2 - V(\phi) - \frac{(\nabla\phi)^2}{6a^2} \tag{2.17}$$

Since the field is assumed to be nearly homogeneous, the spatial derivative can be temporarily neglected.

2.3.1 Slow-roll conditions

It is now possible to quantify the conditions under which the scalar field must adhere to in order to give rise to a period of inflation. In the inflaton model, the dynamics is described by the coupled system of Klein-Gordon and Friedmann equations.

$$H^2 = \frac{1}{3M_{\mathrm{Pl}}^2}\left[\frac{1}{2}\dot{\phi}^2 + V\right] \tag{2.18}$$

$$\ddot{\phi} + 3H\dot{\phi} = -\frac{dV}{d\phi} \tag{2.19}$$

These equations can be combined for the calculation of the slow-roll parameters. In fact, substituting the second one into the time derivative of the first one we get

[2] The use of FRW metric should also determine homogeneity of the field ($\phi = \phi(t)$). For now the spatial derivatives will be left (even if negligible), in order to allow slight fluctuations of the scalar field, which will be essential to describe the origin of inhomogeneities.

$$\dot{H} = -\frac{1}{2}\frac{\dot{\phi}^2}{M_{\rm Pl}^2} \tag{2.20}$$

and then

$$\varepsilon = -\frac{\dot{H}}{H^2} = \frac{\frac{3}{2}\dot{\phi}^2}{\frac{1}{2}\dot{\phi}^2 + V} \tag{2.21}$$

The condition $\varepsilon \ll 1$ is satisfied only if the kinetic energy density $\frac{1}{2}\dot{\phi}^2$ is small compared to the potential energy density V. In other words, the field is slowly rolling down its potential. In this regime, the pressure 2.17 and energy 2.16 densities can be combined to the nominal equation of state for the quasi-de Sitter spacetime ($P = -\rho$).

Now

$$\eta = \frac{\dot{\varepsilon}}{H\varepsilon} = 2\frac{\ddot{\phi}}{H\dot{\phi}} - 2\frac{\dot{H}}{H^2} \tag{2.22}$$

and, if $\varepsilon, \eta < 1$, then

$$\delta \equiv \eta - \varepsilon = -\frac{\ddot{\phi}}{H\dot{\phi}} \ll 1 \tag{2.23}$$

These considerations allow to simplify the Klein-Gordon and Friedmann equations:

$$H^2 \simeq \frac{V}{3M_{\rm Pl}^2} \tag{2.24}$$

$$3H\dot{\phi} \simeq -V_{,\phi} \tag{2.25}$$

where $V_{,\phi} = dV/d\phi$. Slow-roll parameters now purely depend on the potential energy density:

$$\varepsilon \simeq \frac{M_{\rm Pl}^2}{2}\left(\frac{V_{,\phi}}{V}\right)^2 \tag{2.26}$$

$$\eta \simeq M_{\rm Pl}^2 \frac{V_{,\phi\phi}}{V} \tag{2.27}$$

In order for these parameters to be smaller than unity, limits on the choice of the potential must be posed so that its slope does not exceed certain values.

It is useful for the following to define some new slow-roll parameters (ε_V, η_V) that depend solely on the potential, exactly in the manner defined by equations 2.26 and 2.27, so that they coincide with the usual Hubble slow-roll parameters when the slow-roll approximation is valid.

2.3.2 Chaotic inflationary potential

As an example, a very simple inflation model will now be presented. Although excluded by CMB observations [2], this model remains useful for a quantitative analysis of slow-roll conditions. Thus, single-field inflation will be driven by a mass term in the potential:

$$V(\phi) = \frac{1}{2}m^2\phi^2 \tag{2.28}$$

The slow-roll parameters for this potential are:

$$\varepsilon_V = \eta_V = 2\left(\frac{M_{\mathrm{Pl}}}{\phi}\right)^2 \tag{2.29}$$

The value of the field at the end of inflation can be found by imposing the slow-roll condition $\varepsilon_V < 1$:

$$\phi > \sqrt{2}M_{\mathrm{Pl}} \equiv \phi_e \tag{2.30}$$

and, using equation 2.21 together with the condition $N > 70$, one can trace back the field value at the beginning of inflation:

$$\begin{aligned} N = \int_{a_i}^{a_e} d\ln a = \int_{t_i}^{t_e} H(t)dt = \int_{\phi_i}^{\phi_e} \frac{H}{\dot{\phi}}d\phi \simeq \int_{\phi_i}^{\phi_e} \frac{d\phi}{M_{\mathrm{Pl}}}\frac{1}{\sqrt{2\varepsilon_V}} = \\ = \left.\frac{\phi^2}{4M_{\mathrm{Pl}}^2}\right|_{\phi_e}^{\phi_i} = \frac{\phi_i^2}{4M_{\mathrm{Pl}}^2} - \frac{1}{2} > 70 \quad \Longrightarrow \quad \phi_i > 2\sqrt{70}M_{\mathrm{Pl}} \simeq 15M_{\mathrm{Pl}} \end{aligned} \tag{2.31}$$

It is worth noting that all these field values are super-Planckian.

From equations 2.24 and 2.25 it is also possible to infer an initial value for the field derivative:

$$\dot{\phi}_i = -\frac{V_{,\phi}(\phi_i)}{V(\phi_i)} \tag{2.32}$$

Given all this preliminary information, a numerical calculation can be carried out, in order to solve equations 2.18 and 2.19 in the domain where the slow-roll approximation holds. This has been performed with the software Wolfram Mathematica, using equations 2.18 and 2.19 as functions of N, supposing a scalar field mass $m = 7 \times 10^{-6}$ (M_{Pl} units, that is roughly 10^{13}GeV) and using the initial point $\phi_i = 16.5$ (M_{Pl} units).

The calculation revealed that the slow-roll condition, under the aforementioned assumptions, is valid up to the value $N = 68$. Figure 2.1 clearly shows the slowly varying field as it approaches the point of minimum potential in $\phi = 0$. Figure 2.2 shows the effective shrinking of the comoving

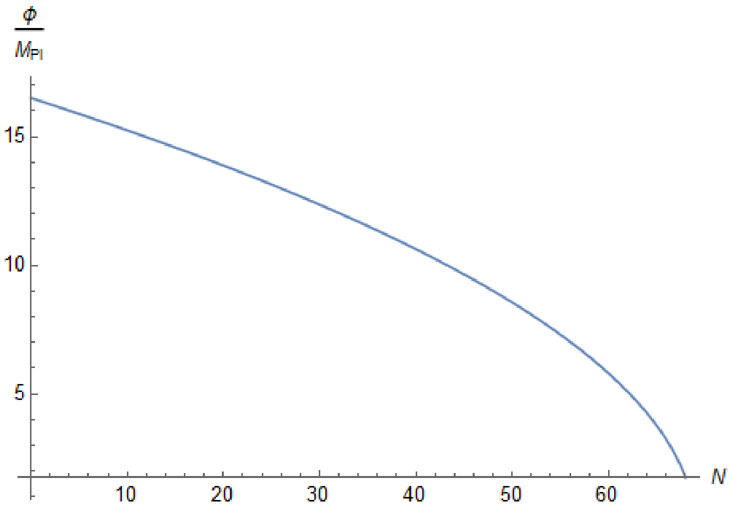

Figure 2.1: *Plot of the scalar field ϕ as function of N in the quadratic potential scalar field inflation.*

Hubble sphere $R_H = 1/aH$ as long as the slow-roll condition holds, as shown in figure 2.3. Finally, in figure 2.4, it can be observed that the Hubble rate remains almost constant (slightly decreasing, as required by the graceful exit) throughout the entire evolution of inflation.

It is possible to verify that an inflation model of this type possesses a smooth graceful exit towards the Friedmann universe. For the sake of brevity the complete calculation will be omitted here, but can be retrieved in the reference [9].

$$\ddot{\phi} + 3H\dot{\phi} = -m^2\phi \tag{2.33}$$

As the scalar field drops below the Planckian value, it begins to oscillate (equation 2.33)[3], giving birth to a stage where the universe begins to expand similarly to the matter-dominated phase. This condensate of massive scalar particles must eventually be converted into the particles of the Standard Model, transferring all the acquired kinetic energy. Such process is called **reheating**.

2.4 Reheating

With the accelerated expansion stage having ended, no mechanisms can amplify the microscopic, high energy effects of the inflaton decay up to cosmological scales, thus making the impact of the reheating era hardly accessible by

[3]The equation is exact when using the mass potential, but any potential can be approximated by the mass potential around its minimum.

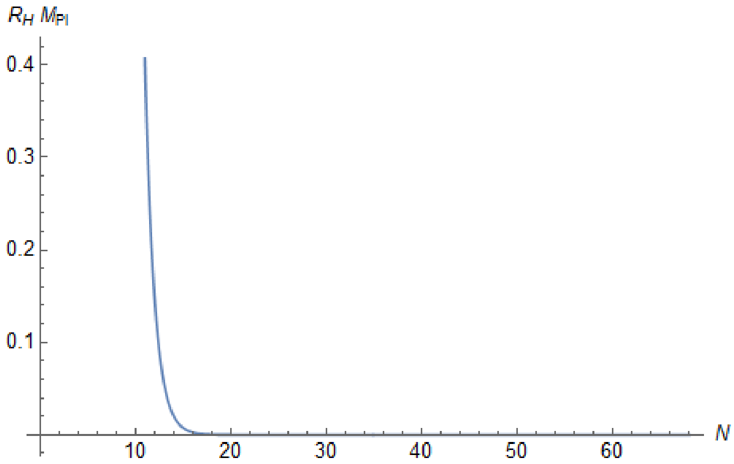

Figure 2.2: *Plot of the comoving Hubble radius R_H as function of N in the quadratic potential scalar field inflation.*

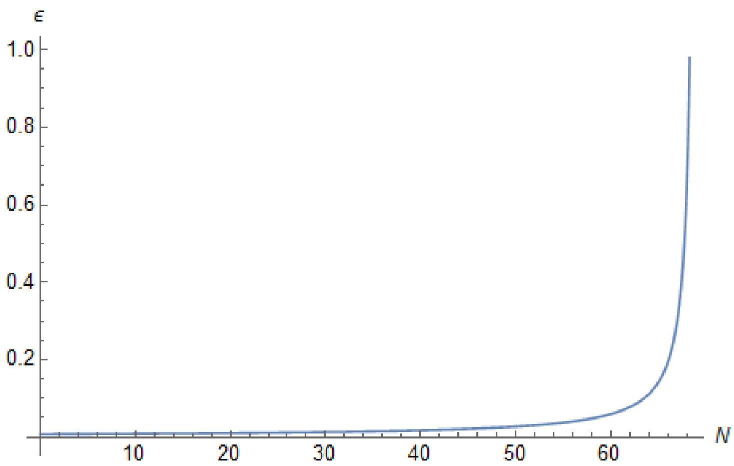

Figure 2.3: *Plot of the potential slow-roll parameter ε as function of N in the quadratic potential scalar field inflation.*

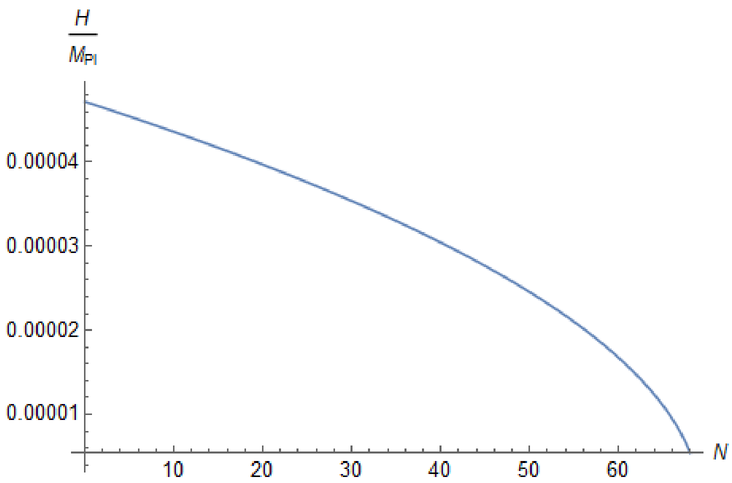

Figure 2.4: *Plot of the Hubble rate as function of N in the quadratic potential scalar field inflation.*

our observation possibilities. Furthermore, inflaton decay crucially depends on the choice of the particle physics theory beyond Standard Model. Nevertheless, general features of the reheating process can be outlined, providing us with some selection criteria among the multiple possibilities.

First of all, the continuity equation for the inflaton's energy density can be modified in order to include a parameter accounting for the inflaton decay rate:

$$\dot{\rho}_\phi + 3H\rho_\phi = -\Gamma_\phi \rho_\phi \tag{2.34}$$

After that, one can consider the simplest coupling between the inflaton and some general scalar χ or spinor ψ field:

$$\Delta L_{\text{int}} = -g\phi\chi^2 - h\phi\bar{\psi}\psi \tag{2.35}$$

The decaying rates of the inflaton field into $\chi\chi$ and $\psi\bar{\psi}$ pairs are determined by the coupling constants g and h:

$$\Gamma_\chi = \frac{g^2}{8\pi m} \qquad \Gamma_\psi = \frac{h^2 m}{8\pi} \tag{2.36}$$

It is possible to show [9] that, for $m \ll M_{\text{Pl}}$, the maximum value for Γ_χ is much higher than the highest possible value for Γ_ψ. Therefore, bosons are created earlier than fermions, well ahead than thermal equilibrium. For this reason, this fast decay is called **preheating**.

Eventually, final particles will thermalize at a new temperature determined by [2]:

$$\rho_R = \frac{\pi^2}{30} g_*(T_R) T_R^4 \tag{2.37}$$

where ρ_R is the energy density at the end of the reheating epoch. At least, this temperature must be larger than 1MeV, in order to allow BBN.

CHAPTER

3

INFLATION: PERTURBATIONS

Up to this point in this thesis work, the universe has been treated as perfectly homogeneous. However, even a cursory visual observation of the space around us reveals that this is not entirely true. The presence of large-scale structures such as galaxies and clusters interspersed with cosmic voids represents a significant deviation from perfect homogeneity. Moreover, sufficiently precise observations of the CMB indicate that such inhomogeneities were present, albeit to a lesser extent, even in the primordial universe. This does not invalidate the work done so far, as the properties of homogeneity and isotropy of the universe are still preserved on sufficiently large spatial scales. Consequently, the approach cosmologists have used to describe the formation and evolution of such inhomogeneities is to apply perturbation theory around the Friedmann metric. For fluctuations on scales smaller than the Hubble radius, a Newtonian treatment of perturbations is more than sufficient, whereas for the study of perturbations on larger scales, or for relativistic fluids, it becomes necessary to use perturbation theory in general relativity.

Gravitational instability is a mechanism that excellently describes the formation and evolution of the large-scale structures observed today, although it requires a fundamental contribution from dark matter. The advantage remains that the macroscopic behavior of the dark matter fluid depends little on its microscopic properties, which are currently unknown. Whatever the approach used to study the fluctuations, the problem concerning their origin, namely the problem of initial conditions, remains open. Assuming that the observed perturbations originated from a perfectly homogeneous background, no classical theory can describe such a spontaneous breaking of homogeneity. A quantum theory is necessary.

At this point, inflation plays a fundamental role. One of the most notable aspects of inflation is that it provides a natural mechanism for the creation of primordial density fluctuations, which constitute the initial conditions for subsequent perturbative evolution. It is worth emphasizing that the theory of inflation was not initially devised to produce such fluctuations, but their origin was instead a natural consequence of the quantum-mechanical treatment carried out by Professor V. Mukhanov and Professor G. Chibisov in 1980.

In this chapter, the theory of perturbations in general relativity will be outlined, followed by its application to inflation. Subsequently, the inflaton field will be quantized, thus allowing the spectrum of quantum fluctuations to be recovered.

3.1 Linear perturbations

Perturbation theory on GR is conceptually straightforward. We write the metric and the energy-momentum tensor as:

$$g_{\mu\nu}(\eta, \mathbf{x}) = \bar{g}_{\mu\nu} + \delta g_{\mu\nu}(\eta, \mathbf{x}) \tag{3.1}$$

$$T_{\mu\nu}(\eta, \mathbf{x}) = \bar{T}_{\mu\nu} + \delta T_{\mu\nu}(\eta, \mathbf{x}) \tag{3.2}$$

where the bar denotes the homogeneous background value. The conceptual part is the only one simple in this theory. From this point, calculations can become lengthy and involved. For the purpose of this thesis, I won't reproduce them all, and I will refer to the literature for the unreported mathematical steps. The purpose is to expand the energy conservation equations and Einstein equations to linear order.

3.1.1 Metric perturbations

Here, $\bar{g}_{\mu\nu}$ is the flat FRW metric. It is possible to perform a scalar-vector-tensor decomposition to the perturbed spacetime:

$$ds^2 = a^2(\eta)\left[-(1+2A)d\eta^2 + 2B_i dx^i d\eta + (\delta_{ij} + 2E_{ij})\, dx^i\, dx^j\right] \tag{3.3}$$

where A, B_i and E_{ij} are function of space and conformal time. These functions can be further decomposed:

$$B_i = \underbrace{\partial_i B}_{\text{scalar}} + \underbrace{\hat{B}_i}_{\text{vector}} \tag{3.4}$$

$$E_{ij} = \underbrace{C\delta_{ij} + \partial_{\langle i}\partial_{j\rangle}E}_{\text{scalar}} + \underbrace{\partial_{(i}\hat{E}_{j)}}_{\text{vector}} + \underbrace{\hat{E}_{ij}}_{\text{tensor}} \tag{3.5}$$

where

$$\partial_{\langle i}\partial_{j\rangle}E \equiv \left(\partial_i\partial_j - \frac{1}{3}\delta_{ij}\nabla^2\right)E$$
$$\partial_{(i}\hat{E}_{j)} \equiv \frac{1}{2}\left(\partial_i\hat{E}_j + \partial_j\hat{E}_i\right)$$

These hatted quantities are all divergenceless and traceless, i.e. $\partial^i\hat{B}_i = 0$, $\partial^i\hat{E}_i = 0$, $\partial^i\hat{E}_{ij} = 0$ and $\hat{E}^i_i = 0$.

The SVT decomposition is useful because, to the linear order in perturbations, Einstein and conservation equations don't mix scalar, vectors and tensors, so they can be treated independently.

Gauge freedom

In the description of the homogeneous and isotropic background, the choice of the preferred reference frame is fixed by the symmetry properties of the universe. In contrast, in the analysis of perturbations, there is no obvious choice of a preferred coordinate system. This additional degree of freedom leads to the appearance of fictitious perturbative modes. These fictitious modes do not describe actual metric fluctuations but solely reflect the properties of the chosen reference frame.

As example, consider a homogeneous FRW spacetime and make the following spatial coordinate change $x^i \to \tilde{x}^i = x^i + \xi^i(\eta, \mathbf{x})$. Assuming ξ^i being small, one can expand $x^i \to \tilde{x}^i = x^i + \xi^i(\eta, \mathbf{x})$, so that the line element becomes

$$ds^2 = a^2(\eta)\left[-d\eta^2 - 2\xi_i' d\tilde{x}^i d\eta + \left(\delta_{ij} - 2\partial_{(i}\xi_{j)}\right) d\tilde{x}^i d\tilde{x}^j\right] \tag{3.6}$$

This corresponds to a perturbation $B_i = -\xi_i'$ and $\hat{E}_i = -\xi_i$. Similarly, consider the time translation $\eta \to \tilde{\eta} = \eta + \xi^o(\eta, \mathbf{x})$. This induces the density perturbation $\delta\rho = -\bar{\rho}'\xi^0$. Of course these are not real fluctuations, but rather fictitious gauge modes. Conversely a real perturbation can be hidden by choosing an appropriate coordinates change.

The above considerations determine the necessity to either fix the gauge or find some quantities that don't change under change of coordinates, namely **gauge invariant** variables.

Gauge-invariant variables

Consider the following coordinate transformation:

$$x^\mu \to \tilde{x}^\mu = x^\mu + \xi^\mu \qquad \text{where} \qquad \begin{aligned} \xi^0 &= T \\ \xi^i &= L^i = \partial^i L + \hat{L}^i \end{aligned} \tag{3.7}$$

where ξ^μ is small. At a given point of spacetime the metric undergoes the following variation:

$$g_{\mu\nu}(x) = \frac{\partial \tilde{x}^\alpha}{\partial x^\mu}\frac{\partial \tilde{x}^\beta}{\partial x^\nu}\tilde{g}_{\alpha\beta}(\tilde{x}) \tag{3.8}$$

Given the specific transformation 3.7:

$$\frac{\partial \tilde{x}^\alpha}{\partial x^\mu} = \begin{pmatrix} \partial\tilde{\eta}/\partial\eta & \partial\tilde{\eta}/\partial x^i \\ \partial\tilde{x}^i/\partial\eta & \partial\tilde{x}^i/\partial x^j \end{pmatrix} = \begin{pmatrix} 1 + T' & \partial_i T \\ (L^i)' & \mathbb{1}_2 + \partial_j L^i \end{pmatrix} \tag{3.9}$$

It is possible to show [2] that in terms of the SVT decomposition this transformation becomes:

$$\begin{aligned} A &\to A - T' - \mathcal{H}T \\ B &\to B + T - L' \\ C &\to C - \mathcal{H}T - \tfrac{1}{3}\nabla^2 L \\ E &\to E - L \end{aligned} \qquad \begin{aligned} \hat{B}_i &\to \hat{B}_i - \hat{L}_i' \\ \hat{E}_i &\to \hat{E}_i - \hat{L}_i \end{aligned} \qquad \hat{E}_{ij} \to \hat{E}_{ij} \tag{3.10}$$

It is immediately apparent that the tensor component is not affected by the change of coordinates. By defining particular combinations of the metric perturbations, the following variables are found that do not transform under coordinate changes:

$$\begin{aligned} \Psi &\equiv A + \mathcal{H}(B - E') + (B + E')' \\ \Phi &\equiv -C + \tfrac{1}{3}\nabla^2 E - \mathcal{H}(B - E') \end{aligned} \qquad \hat{\Phi}_i = \hat{B}_i - \hat{E}_i' \qquad \hat{E}_{ij} \tag{3.11}$$

Gauge fixing

An alternative solution to the gauge problem is to impose some gauge conditions on the metric perturbations, thus removing the additional degrees of freedom introduced by T, L and $\hat{L}^i$ in 3.7. Here are reported some convenient and popular gauges:

Newtonian gauge This gauge is defined by the choice:

$$B = E = 0 \tag{3.12}$$

The line element 3.3 becomes:

$$ds^2 = a^2(\eta)\left[-(1+2\Psi)d\eta^2 + (1-2\Phi)\delta_{ij}dx^i dx^j\right] \tag{3.13}$$

where $A = \Psi$ and $C = -\Phi$. The advantage of this choice is that the metric is diagonal, thereby simplifying the calculations, and resembles the weak field limit in GR, with Ψ representing the gravitational potential.

Spatially flat gauge In this gauge we set:

$$C = E = 0 \tag{3.14}$$

This will be particularly convenient when studying inflationary perturbations.

Synchronous gauge Here

$$A = B = 0 \tag{3.15}$$

This choice doesn't fix the gauge completely: there exists a class of synchronous coordinate systems. This leads to the appearance of non-physical gauge modes.

3.1.2 Matter perturbations

We consider now the perturbations of the energy-momentum tensor:

$$\begin{aligned}
&T^0_{\ 0} \equiv -\left(\bar{\rho} + \delta\rho\right) \\
&T^0_{\ i} \equiv \left(\bar{\rho} + \bar{P}\right) v_i \equiv q_i \\
&T^i_{\ j} \equiv \left(\bar{P} + \delta P\right) \delta^i_j + \Pi^i_{\ j} \qquad \Pi^i_{\ i} = 0
\end{aligned} \tag{3.16}$$

where v_i is called **bulk velocity** and $\Pi^i_{\ j}$ **anisotropic stress**.

In analogy with the metric, a SVT decomposition is applied to these perturbations: $\delta\rho$ and δP are already scalar quantities, then:

$$\begin{aligned} v_i &= \partial_i v + \hat{v}_i \\ q_i &= \partial_i q + \hat{q}_i \end{aligned} \tag{3.17}$$

and eventually

$$\Pi_{ij} = \partial_{\langle i}\partial_{j\rangle}\Pi + \partial_{(i}\hat{\Pi}_{j)} + \hat{\Pi}_{ij} \tag{3.18}$$

As with the metric, matter perturbations depend on the choice of the coordinate system.

Gauge-invariant variables

Performing the generic change of coordinates 3.7 leads to the following transformation to the energy-momentum tensor perturbations:

$$\begin{aligned} \delta\rho &\to \delta\rho - \bar{\rho}' T \\ \delta P &\to \delta P - \bar{P}' T \\ q_i &\to q_i + \left(\bar{\rho} + \bar{P}\right) L_i' \\ v_i &\to v_i + L_i' \\ \Pi_{ij} &\to \Pi_{ij} \end{aligned} \tag{3.19}$$

As before, specific combinations of the matter perturbations can be defined in order to be independent of the chosen coordinate system:

$$\bar{\rho}\Delta \equiv \delta\rho + \bar{\rho}'\,(v + B) \tag{3.20}$$

$$\zeta \equiv -C + \frac{1}{3}\nabla^2 E + \mathcal{H}\frac{\delta\rho}{\bar{\rho}'} \tag{3.21}$$

$$\mathcal{R} \equiv -C + \frac{1}{3}\nabla^2 E - \mathcal{H}\,(v + B) \tag{3.22}$$

The quantity Δ is called **comoving density contrast** and the quantities ζ and $\mathcal{R}$ are called **curvature perturbations**.They are not independent, but obey the following relation:

$$\zeta = \mathcal{R} - \frac{\mathcal{H}}{\bar{\rho}'}\bar{\rho}\Delta \tag{3.23}$$

Gauge fixing

As before, it is possible to eliminate the extra degrees of freedom by setting some of the perturbations to zero:

Uniform density gauge In this gauge the total density perturbation vanishes:

$$\delta\rho = 0 \tag{3.24}$$

Comoving gauge Similarly, the scalar momentum density can be set to zero:

$$q = 0 \tag{3.25}$$

3.1.3 Conservation and Einstein equations

The task is now to obtain the evolution equations for the previously defined perturbations. The metric is governed by Einstein equations while the matter follows the the conservation of the energy-momentum tensor. They need to be expanded to give the linearized equations of motion of perturbations. Many details of this calculation will be omitted, skipping directly to the result, but they can be found in the reference [2].

The most convenient method for performing this analysis is in the fixed Newtonian gauge. Because this gauge involves the invariant quantities Φ and Ψ one can easily recast all equations for any reference frame.

Conservation equations

Here the equation $\nabla^\mu T_{\mu\nu} = 0$ will be linearized. Considering that

$$\nabla_\mu T^\mu_{\ \nu} = \partial_\mu T^\mu_{\ \nu} + \Gamma^\mu_{\mu\alpha} T^\alpha_{\ \nu} - \Gamma^\alpha_{\mu\nu} T^\mu_{\ \alpha} \tag{3.26}$$

we need the following perturbed connection coefficient:

$$\begin{aligned}
\Gamma^0_{00} &= \mathcal{H} + \Psi' \\
\Gamma^0_{i0} &= \partial_i \Psi \\
\Gamma^i_{00} &= \delta^{ij}\partial_j \Psi \\
\Gamma^0_{ij} &= \mathcal{H}\delta_{ij} - \left[\Phi' + 2\mathcal{H}(\Phi + \Psi)\right]\delta_{ij} \\
\Gamma^i_{j0} &= \left[\mathcal{H} - \Phi'\right]\delta^i_j \\
\Gamma^i_{jk} &= -2\delta^i_{(j}\partial_{k)}\Phi + \delta_{jk}\delta^{il}\partial_l \Phi
\end{aligned} \tag{3.27}$$

After long work, the linearized continuity ($\nu = 0$) and Euler ($\nu = i$) are obtained:

$$\begin{aligned}
\delta' &= -\left(1 + \frac{\bar{P}}{\bar{\rho}}\right)(\theta - 3\Phi') - 3\mathcal{H}\left(\frac{\delta P}{\delta\rho} - \frac{\bar{P}}{\bar{\rho}}\right)\delta \\
\theta' &= -\left(\mathcal{H} + \frac{\bar{P}'}{\bar{\rho} + \bar{P}}\right)\theta - \frac{1}{\bar{\rho} + \bar{P}}\left(\nabla^2\delta P - \frac{2}{3}\nabla^4\Pi\right) - \nabla^2\Psi
\end{aligned} \tag{3.28}$$

where $\delta \equiv \delta\rho/\bar{\rho}$ is called **density contrast** and $\theta \equiv \partial_i v^i$ is the **velocity divergence**.

Einstein equations

Following the same approach, the equations $G_\mu = 8\pi G T_{\mu\nu}$ are perturbed. The process involves the Einstein tensor $G_{\mu\nu} \equiv R_{\mu\nu} - \frac{1}{2} R g_{\mu\nu}$ and as a consequence the Ricci tensor and scalar:

$$\begin{aligned} R_{\mu\nu} &= \partial_\lambda \Gamma^\lambda_{\mu\nu} - \partial_\nu \Gamma^\lambda_{\mu\lambda} + \Gamma^\lambda_{\lambda\rho}\Gamma^\rho_{\mu\nu} - \Gamma^\rho_{\mu\lambda}\Gamma^\lambda_{\nu\rho} \\ R &= g^{\mu\nu} R_{\mu\nu} \end{aligned} \tag{3.29}$$

which won't be calculated here. The result are the linearized equations for the metric evolution:

$$\begin{aligned} \nabla^2\Phi - 3\mathcal{H}\left(\Phi' + \mathcal{H}\Psi\right) &= 4\pi G a^2 \delta\rho \\ -\left(\Phi' + \mathcal{H}\Psi\right) &= 4\pi G a^2 q \\ \Phi - \Psi &= 8\pi G a^2 \Pi \\ \Phi'' + \mathcal{H}\Psi' + 2\mathcal{H}\Phi' + \frac{1}{3}\nabla^2(\Psi - \Phi) + \left(2\mathcal{H}' + \mathcal{H}^2\right)\Psi &= 4\pi G a^2 \delta P \end{aligned} \tag{3.30}$$

The Einstein equations, together with the Euler and continuity equations, form a closed system that needs to be specialized for each fluid component of the universe (photons, baryons, neutrinos, cold dark matter, inflaton) and completed with the equation of state and the speed of sound for each of them. Naturally, the complete resolution of this system requires the specification of initial conditions for the perturbations, a task comprehensively accomplished by the quantization of the inflationary scalar field, which will be addressed in the following sections. The problem of initial conditions is, however, simplified by the fact that all scales of interest for current observations were outside the Hubble radius. In the superhorizon limit of the conservation and Einstein equations, the fluctuations of the various components are related by a very simple relation:

$$\delta_\gamma = \delta_\nu = \frac{4}{3}\delta_c = \frac{4}{3}\delta_b = -2\Phi_i \tag{3.31}$$

where all quantities are functions of k.

Consequently, the initial conditions are determined by providing the initial value for the gravitational potential, which, in the radiation-dominated era, is in turn related to the curvature perturbation by the relation:

$$\Phi_i(\mathbf{k}) = \frac{2}{3}\mathcal{R}_i(\mathbf{k}) \tag{3.32}$$

so that the amplitude of all fluctuations is completely determined by $\mathcal{R}_i$. This quantity is commonly specified through the "primordial power spectrum," which is assumed to have the following form:

$$\mathcal{P}_{\mathcal{R}}(k, t_i) = Ak^n \tag{3.33}$$

where A and n are constants.

In the next section, the details of the quantum mechanical treatment of the inflaton field will be shown, and it will be demonstrated that inflation naturally predicts a scale-invariant spectrum with $n \approx 1$.

3.2 Quantum initial conditions

Recall from the previous chapter that the inflaton field dominates the energy density of the universe during inflation and consequently controls its temporal evolution. In other words, the value of the field ϕ indicates the remaining time before inflation ends. For this reason, ϕ is often referred to as the "clock" of inflation. However, in quantum mechanics, arbitrarily precise timing is rendered impossible by the non-commutativity between the field and its momentum $\dot{\phi}$ (Heisenberg uncertainty principle). The inflaton will therefore have position-dependent fluctuations $\delta\phi(t, \mathbf{x})$, such that some regions of space will end their inflationary phase earlier than others. These regions will begin their Friedmann expansion sooner and will dilute, resulting in areas of lower density. The portions of space that inflate longer will thus have higher densities. Figure 3.1, taken from reference [2], beautifully and intuitively illustrates the mechanism of fluctuation production.

3.2.1 Classical equations

The dynamics of the inflaton field is determined by the action

$$S = \int d^4x\sqrt{-g}\left(-\frac{1}{2}g^{\mu\nu}\partial_\mu\phi\partial_\nu\phi - V(\phi)\right) \tag{3.34}$$

The equation of motion associated with this action will couple the inflaton fluctuations $\delta\phi$ with the metric fluctuations $\delta g_{\mu\nu}$ in a gauge dependent manner. It will be convenient to perform this analysis in the spatially flat gauge, where the line element (with only scalar perturbations) is:

$$ds^2 = a^2(\eta)\left[-\left(1+2A\right)d\eta^2 + 2\partial_i B dx^i d\eta + \delta_{ij}dx^i dx^j\right] \tag{3.35}$$

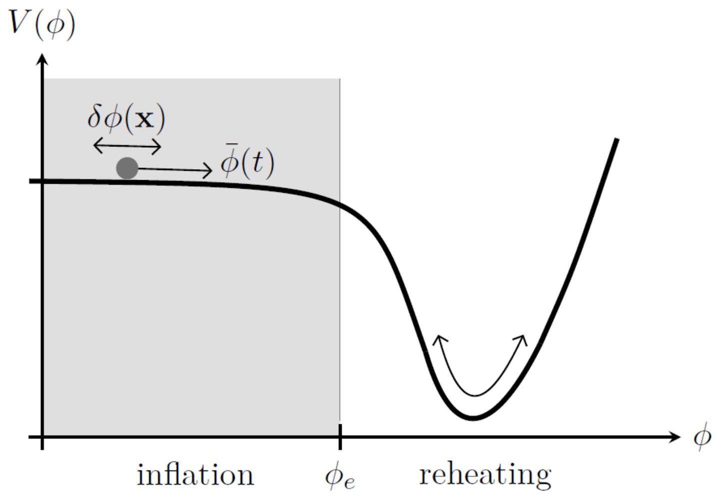

Figure 3.1: *Quantum fluctuations around the background field ϕ.*

Varying of the action 3.34 leads to the Klein-Gordon equation

$$\frac{1}{\sqrt{-g}}\partial_\mu\left(\sqrt{-g}g^{\mu\nu}\partial_\nu\phi\right) = V_{,\phi} \tag{3.36}$$

At first order the inverse perturbed metric is:

$$\begin{aligned} g^{00} &= -a^{-2}\left(1-2A\right) \\ g^{0i} &= a^{-2}\partial_i B \\ g^{ij} &= a^{-2}\delta_{ij} \end{aligned} \tag{3.37}$$

and $\sqrt{-g} = a^4\left(1+A\right)$. Inserting this metric and the perturbed scalar field $\phi = \bar{\phi} + \delta\phi$ into 3.36, the result is:

$$\delta\phi'' + 2\mathcal{H}\delta\phi' - \nabla^2\delta\phi = \left(A' + \nabla^2 B\right)\bar{\phi}' - 2a^2 V_{,\phi}A - a^2 V_{,\phi\phi}\delta\phi \tag{3.38}$$

Now, Einstein equations are necessary to close the system. First of all, a variation of action 3.34 with respect to the metric gives the energy-momentum tensor for inflaton:

$$T_{\mu\nu} = \partial_\mu\phi\partial_\nu\phi - g_{\mu\nu}\left(\frac{1}{2}g^{\alpha\beta}\partial_\alpha\phi\partial_\beta\phi + V(\phi)\right) \tag{3.39}$$

Subsequently, its perturbation is ready to be calculated:

$$\begin{aligned} \delta T^0{}_0 &= -\left[a^{-2}\left(\bar{\phi}'\delta\phi' - \left(\bar{\phi}'\right)^2 A\right) + V_{,\phi}\delta\phi\right] \\ \delta T^0{}_i &= -\frac{\bar{\phi}'}{a^2}\partial_i\delta\phi \end{aligned} \tag{3.40}$$

Next we move to the perturbed Einstein tensor:

$$\begin{aligned} \delta G^0{}_i &= -\frac{2\mathcal{H}}{a^2}\partial_i A \\ \delta G^0{}_0 &= \frac{2\mathcal{H}}{a^2}\left(3\mathcal{H}A + \nabla^2 B\right) \end{aligned} \tag{3.41}$$

It is now possible to compute the 0i and 00 Einstein equations. From the former one, A can be eliminated in favour of $\delta\phi$:

$$\delta G^0{}_i = -\frac{2\mathcal{H}}{a^2}\partial_i A = 8\pi G \delta T^0{}_i = -8\pi G \frac{\bar{\phi}'}{a^2}\partial_i \delta\phi \tag{3.42}$$

from which

$$A = 4\pi G \frac{\bar{\phi}'}{\mathcal{H}}\delta\phi = \varepsilon \frac{\mathcal{H}}{\bar{\phi}'}\delta\phi \tag{3.43}$$

From the latter, we can eliminate B:

$$\begin{aligned} \delta G^0{}_0 = \frac{2\mathcal{H}}{a^2}\left(3\mathcal{H}A + \nabla^2 B\right) &= 8\pi G \delta T^0{}_0 \\ &= -8\pi G \left[a^{-2}\left(\bar{\phi}'\delta\phi' - \left(\bar{\phi}'\right)^2 A\right) + V_{,\phi}\delta\phi\right] \end{aligned} \tag{3.44}$$

with the help of the background equation

$$\bar{\phi}'' + 2\mathcal{H}\bar{\phi}' + a^2 V_{,\phi} \tag{3.45}$$

we get

$$\nabla^2 B = -\varepsilon \frac{\mathcal{H}}{\bar{\phi}'}\left(\delta\phi' + (\delta - \varepsilon)\mathcal{H}\delta\phi\right) \tag{3.46}$$

The substitution of 3.43 and 3.46 into 3.38 gives the following closed form equation for inflation fluctuations:

$$\delta\phi'' + 2\mathcal{H}\delta\phi' - \nabla^2\delta\phi = \left[(3 + 2\varepsilon - \delta)(\varepsilon - \delta) - \frac{\delta'}{\mathcal{H}}\right]\mathcal{H}^2\delta\phi \tag{3.47}$$

This equation can be greatly simplified by defining the variable:

$$f \equiv a\delta\phi \tag{3.48}$$

The result is the so called **Mukhanov-Sasaki equation**:

$$f'' + \left(k^2 - \frac{z''}{z}\right) f = 0 \qquad \text{where} \qquad z \equiv \frac{a\bar{\phi}'}{\mathcal{H}} \tag{3.49}$$

Despite the appearance of the slow-roll parameters, we have *not* made any slow-roll approximation. Therefore, this equation doesn't contain any approximations and is valid on all scales.

For the quantization procedure that will be treated in the next sections, we well make also use of the action from which 3.49 arises:

$$S_2 = \frac{1}{2}\int d\eta d^3x \left[(f')^2 - (\nabla f)^2 + \frac{z''}{z} f^2 \right] \tag{3.50}$$

3.2.2 Classical solutions

Equation 3.49 is the equation of a harmonic oscillator with time dependent frequency:

$$\omega^2(\eta, k) = k^2 - \frac{z''}{z} \tag{3.51}$$

In slow roll conditions H and $d\bar{\phi}/dt$ are almost constants so that

$$\frac{z''}{z} \approx \frac{a''}{a} \approx 2\mathcal{H}^2 \tag{3.52}$$

and the inverse of z''/z is a measure of the Hubble radius.

Solutions to the Mukhanov-Sasaki equation will be reported here in two cases:

- At early times, all modes were inside the horizon. Taking the limit $k^2 \gg |z''/z|$ equation 3.49 becomes:

  $$f'' + k^2 f = 0 \tag{3.53}$$

  This equation has solutions

  $$f \propto e^{\pm ik\eta} \tag{3.54}$$

  The amplitude of these oscillations will be determined in the quantum treatment of fluctuations.

- As microscopical scales are inflated outside the physical Hubble radius H^{-1} (i.e. the comoving Hubble radius $\mathcal{H}^{-1}$ shrinks), the evolution changes. In the limit $k^2 \ll |z''/z|$, equation 3.49 reads:

  $$f'' - \frac{z''}{z} f = 0 \tag{3.55}$$

  which has a decaying solution $f \propto z^{-2}$ and a growing solution $f \propto z$.

It is possible to show that

$$\mathcal{R} = -\frac{\mathcal{H}}{\bar{\phi}'}\delta\phi = -\frac{f}{z} \xrightarrow{k \ll \mathcal{H}} \text{const} \tag{3.56}$$

so we infer that the growing solution on large scales represents a frozen perturbation.

3.2.3 Quantum fluctuations

The Fourier modes of the scalar field perturbations satisfy the equation of a harmonic oscillator. With this in mind, an EFT treatment of inflation seems natural. It will be most convenient to perform this quantization using Heisenberg picture, where operators vary in time, while states are time independent. An operator $\hat{O}$ satisfies the evolution equation

$$\frac{d\hat{O}}{dt} = \frac{i}{\hbar}\left[\hat{H}, \hat{O}\right] \tag{3.57}$$

where $\hat{H}$ is the Hamiltonian

$$\hat{H} = \frac{1}{2}\hat{p}^2 + \frac{1}{2}\omega^2\hat{q}^2 \tag{3.58}$$

with

$$[\hat{q}, \hat{p}] = i\hbar \tag{3.59}$$

We write the position operator as:

$$\hat{q}(t) = q(t)\hat{a}(t_i) + q^*(t)\hat{a}^\dagger(t_i) \tag{3.60}$$

where the complex mode function $q(t)$ satisfies

$$\ddot{q} + \omega^2(t)q = 0 \tag{3.61}$$

The annihilation operator $\hat{a}(t_i)$ and its associated vacuum state $|0\rangle$ depend on the choice of initial time t_i. We will see that this choice determines a series of conceptual problems.

Inserting 3.60 into 3.59, we get:

$$[\hat{q}, \hat{p}] = (q\dot{q}^* - \dot{q}q^*)\left[\hat{a}, \hat{a}^\dagger\right] = i\hbar \tag{3.62}$$

Being $\left[\hat{a}, \hat{a}^\dagger\right] = 1$, we obtain the mode function normalization

$$q\dot{q}^* - \dot{q}q^* = i\hbar \tag{3.63}$$

To completely fix the mode function $q(t)$, it is necessary to impose a second condition. We take the initial condition to be the ground state of the fixed-frequency oscillator and then use the equation of motion with a time-dependent frequency to evolve these fluctuations forward in time. We write a general ground state as:

$$q(t) = r(t)e^{is(t)} \tag{3.64}$$

equation 3.63 implies:

$$\dot{s} = -\frac{\hbar}{2r^2} \tag{3.65}$$

In order to find the solution, we have to minimize the vacuum expectation value:

$$\begin{aligned}
\langle 0| \hat{H} |0\rangle &= \frac{1}{2}\left(|\dot{q}|^2 + \omega^2 |q|^2\right) \\
&= \frac{1}{2}\left(\dot{r}^2 + r^2\dot{s}^2 + \omega^2 r^2\right) \\
&= \frac{1}{2}\left(\dot{r}^2 + \frac{\hbar}{4r^2} + \omega^2 r^2\right)
\end{aligned} \tag{3.66}$$

which has a minimum in:

$$\dot{r} = 0 \quad \text{and} \quad 0 = \frac{d}{dr^2}\left(\frac{\hbar}{4r^2} + \omega^2 r^2\right) = -\frac{\hbar}{4\left(r^2\right)^2} + \omega^2 \quad \Longrightarrow \quad r = \sqrt{\frac{\hbar}{2\omega}} \tag{3.67}$$

Inserting back this solution back in 3.65 we get:

$$q(t) = \sqrt{\frac{\hbar}{2\omega}} e^{-i\omega t} \qquad (\omega = \text{const}) \tag{3.68}$$

Using this solution as initial condition for equation 3.61 uniquely fixes the expression for the position operator. The explicit solution depends on the form of $\omega(t)$, which for inflation is determined by the evolution of the background.

Field quantization

We will now apply the quantization procedure to the scalar field fluctuations during inflation. Slow-roll approximation will be considered for simplicity so that the Mukhanov-Sasaki equation 3.49 takes the form:

$$f_{\mathbf{k}}'' + \left(k^2 - \frac{2}{\eta^2}\right) f_{\mathbf{k}} = 0 \tag{3.69}$$

The field $f(\eta, \mathbf{x})$ and its conjugate momentum $\pi(\eta, \mathbf{x})$ are now promoted to operators, with commutation rule:

$$\left[\hat{f}(\eta, \mathbf{x}), \hat{\pi}(\eta, \mathbf{x}')\right] = i\delta(\mathbf{x} - \mathbf{x}') \tag{3.70}$$

where $\hbar = 1$. In the Fourier space, the commutation rule becomes:

$$\begin{aligned}\left[\hat{f}_{\mathbf{k}}(\eta), \hat{\pi}_{\mathbf{k}'}(\eta)\right] &= \int d^3x \int d^3x' \left[\hat{f}(\eta, \mathbf{x}), \hat{\pi}(\eta, \mathbf{x}')\right] e^{-i\mathbf{k}\cdot\mathbf{x}} e^{-i\mathbf{k}'\cdot\mathbf{x}'} \\ &= i \int d^3x e^{-i(\mathbf{k}+\mathbf{k}')\cdot\mathbf{x}} \\ &= i(2\pi)^3\delta(\mathbf{k} + \mathbf{k}')\end{aligned} \tag{3.71}$$

As before, we can write the field Fourier components as:

$$\hat{f}_{\mathbf{k}}(\eta) = f_k(\eta)\hat{a}_{\mathbf{k}} + f_k^*(\eta)\hat{a}^\dagger_{-\mathbf{k}} \tag{3.72}$$

where the $-\mathbf{k}$ accounts for the hermiticity of the field operator, and the complex mode function $f_k(\eta)$ solves the classical equation 3.69. Equation 3.63 here becomes:

$$f_k f_k'^* - f_k' f_k^* = i \tag{3.73}$$

and inserting 3.72 into 3.71 we get

$$\left[\hat{a}_{\mathbf{k}}, \hat{a}^\dagger_{\mathbf{k}'}\right] = (2\pi)^3\delta(\mathbf{k} + \mathbf{k}') \tag{3.74}$$

Choice of vacuum

As before, an initial condition has to be imposed in order to uniquely determine the field operator. A common choice is to define the vacuum as the ground state of the Hamiltonian at $\eta \to -\infty$, when all modes where inside the horizon and satisfied the equation of a harmonic oscillator with fixed frequency $\omega_k \to k$. This state as been already calculated (3.68) and the initial condition becomes:

$$\lim_{k\eta \to -\infty} f_k(\eta) = \frac{1}{\sqrt{2k}} e^{-ik\eta} \tag{3.75}$$

The solution of the Mukhanov-Sasaki equation 3.69 with this initial condition is the following:

$$f_k(\eta) = \frac{1}{\sqrt{2k}} \left(1 - \frac{i}{k\eta}\right) e^{-ik\eta} \tag{3.76}$$

which is called the **Bunch-Davies mode function**, and the corresponding state is the **Bunch-Davies vacuum**.

Vacuum fluctuations

It is now time to calculate the statistic fluctuations of the scalar field. The expectation value of the operator $\hat{f}$ vanishes, but its variance determines zero-point fluctuations:

$$\begin{aligned}
&\left\langle \left|\hat{f}\right|^2 \right\rangle = \langle 0| \, \hat{f}(\eta,0)\hat{f}(\eta,0) \, |0\rangle \\
&= \int \frac{d^3k}{(2\pi)^3} \int \frac{d^3k'}{(2\pi)^3} \langle 0| \left(f_k^*(\eta)\hat{a}_{\mathbf{k}} + f_k(\eta)\hat{a}^\dagger_{-\mathbf{k}} \right) \left(f_{k'}(\eta)\hat{a}_{\mathbf{k}'} + f_{k'}^*(\eta)\hat{a}^\dagger_{-\mathbf{k}'} \right) |0\rangle \\
&= \int \frac{d^3k}{(2\pi)^3} \int \frac{d^3k'}{(2\pi)^3} f_k(\eta) f_{k'}^*(\eta) \, \langle 0| \left[\hat{a}_{-\mathbf{k}}, \hat{a}^\dagger_{-\mathbf{k}'} \right] |0\rangle \\
&= \int \frac{d^3k}{(2\pi)^3} \left| f_k(\eta) \right|^2 \\
&= \int d\ln k \frac{k^3}{2\pi^2} \left| f_k(\eta) \right|^2 = \int d\ln k \Delta_f^2(k,\eta)
\end{aligned} \tag{3.77}$$

Substituting the Bunch-Davies mode function for $f = a\delta\phi$, we obtain the power spectrum:

$$\Delta^2_{\delta\phi}(k,\eta) = \frac{\Delta_f^2(k,\eta)}{a^2(\eta)} = \left(\frac{H}{2\pi}\right)^2 \left[1 + (k\eta)^2\right] \overset{k\eta\to 0}{\longrightarrow} \left(\frac{H}{2\pi}\right)^2 \tag{3.78}$$

Primordial power spectrum

The final task is to calculate the observable density fluctuations produced just after inflation. The field perturbation $\delta\phi$ has no longer meaning, having the inflaton converted into the Standard Model particles. The gauge-invariant quantities, however, remain well defined. Therefore, it is convenient to relate the field fluctuation spectrum to these quantities to allow the connection between inflation and the late universe. In particular, the curvature perturbation spectrum $\mathcal{R}$ is used. Recalling relation 3.56 the power spectrum of $\mathcal{R}$ can be written as:

$$\Delta^2_{\mathcal{R}} = \left(\frac{H}{\dot{\phi}}\right)^2 \Delta_{\delta\phi} = \left(\frac{H^2}{2\pi\dot{\phi}^2}\right)^2 \Bigg|_{k=aH} = \frac{1}{8\pi^2\varepsilon} \frac{H^2}{M^2_{\mathrm{Pl}}} \Bigg|_{k=aH} \tag{3.79}$$

where the spectrum has been evaluated at horizon crossing $k = aH$ to introduce a slight scale dependence.

We introduce the spectral index:

$$n_s - 1 \equiv \frac{d\ln \Delta^2_{\mathcal{R}}(k)}{d\ln k} \tag{3.80}$$

so that the primordial spectrum takes the form:

$$\Delta^2_{\mathcal{R}}(k) = A_s \left(\frac{k}{k_*}\right)^{n_s-1} \tag{3.81}$$

Tensor fluctuations

Up to this point, exclusively scalar fluctuations have been considered. Being completely independent, tensor perturbations to the metric can be analyzed separately:

$$ds^2 = a^2(\eta)\left[-d\eta^2 + (\delta_{ij} + h_{ij})\, dx^i dx^j\right] \tag{3.82}$$

Following the same steps of the scalar perturbations, it is possible to show that tensor perturbations satisfy the following equation:

$$h''_{ij} + 2\mathcal{H}h'_{ij} - \nabla^2 h_{ij} = 0 \tag{3.83}$$

which comes from the same action of a scalar field, taken once for each polarization mode:

$$S_2 = \frac{1}{2}\sum_{\lambda=+,\times}\int d\eta d^3x \left[(f'_\lambda)^2 - (\nabla f_\lambda)^2 + \frac{a''}{a} f_\lambda^2\right] \tag{3.84}$$

The resulting power spectrum will be therefore a rescaling of the scalar spectrum:

$$\Delta^2_h(k) = \frac{2}{\pi^2}\left(\frac{H}{M_{\text{Pl}}}\right)^2\Bigg|_{k=aH} \tag{3.85}$$

These tensor perturbations correspond to the production of primordial gravitational waves. Their amplitude can be estimated through the tensor to scalar ratio

$$r = \frac{A_t}{A_s} = 16\varepsilon \tag{3.86}$$

since the the amplitude of scalar fluctuations has been measured.

3.2.4 Evidences and open problems

Most observations related to inflation are comprised of CMB measurements. Increasingly detailed analyses of this radiation can provide a growing number of clues about the details of this primordial phase of the universe's evolution. A very significant piece of evidence supporting inflation is the fact that a nearly featureless spectrum of initial fluctuations evolves, via perturbation theory in GR, into the peaks and valleys of the CMB spectrum. Since the dynamics of these fluctuations are well known and established, constraints on the primordial power spectrum can be set from CMB observations. A very important prediction of inflation is that of a nearly scale-invariant spectrum of perturbations, which is strongly compatible with current measurements, attributing a value of [1]

$$n_s = 0.9665 \pm 0.0038 \tag{3.87}$$

to the spectral index.

Experimental research is currently focused on investigating the aspects of inflation more deeply, including comparing results from different types of measurements. For instance, the detection of the tensor component of primordial fluctuations can provide very direct evidence, such as the energy scale of inflation, since the universe has always been transparent to primordial gravitational waves from their production onwards.

Theoretical research, at the same time, is concentrated on a wide range of fundamental issues raised by inflation, as it provides a window into physics at energy scales much higher than those of standard models. Quantum gravitational effects or the presence of conditions different from those predicted by single-field slow-roll inflation can be considered, along with a necessary analysis of the reheating phase. Following this, we will address a particular open problem of inflation, which has been the fundamental motivation for this thesis work.

3.2.5 The trans-Planckian problem

Regardless of who we are or where we come from,
we were all once super-Planckian fluctuations.

In section 3.2.3 we have seen that one of the most accepted choices for the initial condition for inflation fluctuations is the Bunch-Davies vacuum. It minimizes the Hamiltonian, in consistence with the uncertainty principle, and leads to a scale-invariant spectrum. However, one could argue [4] that an initial condition taken at $\eta \to -\infty$ is a too strong condition. Moreover, this choice leads to consider perturbation modes with $k \to 0$, that is modes with infinite energy. This means that modes evolution goes through a trans-Planckian regime, about which there is no robust theoretical foundation.

A typical way to overcome this problem is by introducing an initial time $\bar{\tau}_k$ such that the mode evolution begins only once its energy has dropped to a safe value where GR can be reliably used. This corresponds to introducing a cut-off scale Λ, with $H < \Lambda \leq M_{\rm Pl}$, such that

$$\bar{\eta}_k \simeq -\frac{\Lambda}{kH} \tag{3.88}$$

This choice leads to a different prescription on annihilation operators and vacuum state, now defined as:

$$\hat{a}_k(\bar{\eta}_k)\,|0, \bar{\eta_k}\rangle = 0 \tag{3.89}$$

Vacuum states defined in this way are called α-**vacua**.

Using α-vacua leads to a different expression for the primordial tensor spectrum [3]:

$$\mathcal{P}_h(k) = \frac{16H^2}{\pi M_{\rm Pl}^2}\left[1 + \frac{H}{\Lambda}\sin\left(\frac{2\Lambda}{H}\right) + \dots\right] \tag{3.90}$$

A slight departure from the standard spectrum has been induced, with an oscillating feature that is subdominant since $\Lambda \gg H$.

Despite this approach, still the question remains unanswered of what are the dynamics of the fluctuations in the trans-Planckian regime.

CHAPTER

4 INITIAL CONDITIONS: A STOCHASTIC MODEL

The general purpose of this thesis is to study the impact that different models for the inflation can have on the primordial spectrum, on the CMB spectrum and on the cosmological observables.

A particular focus is aimed at a model for the description of the evolution of inflation fluctuations in the trans-Planckian regime, developed by doctor Mattia Cielo and professors Gianpiero Mangano and Ofelia Pisanti in the reference [4]. In this paper, the authors suggest that the evolution of tensor perturbations in the high energy regime above some energy scale Λ can be effectively described by adding a stochastic source term with zero mean to the evolution equations, which is due to the interaction of modes with the underlying background of fluctuations due to quantum gravity nonlinear effects. They also propose a scenario to model this background source term, which will be presented in the following sections.

4.1 Limits of the perturbation theory

We have not yet a full theory of gravity in its quantum regime. Nevertheless, inflation involves energies somehow close to the Planck scale: recall from section 2.3.2 that during inflation the Hubble rate is just five orders of magnitude below the Planck mass while the initial field value can reach up 15 times the Planck energy. Moreover, inflation will produce fluctuations the size of which can be smaller than the Planck length. As a consequence, some considerations [4] must be made in order to make assumptions on the dynamics of such fluctuations:

- we expect linear approximation to be not an appropriate one when modes experience the high energy scale Λ regime since nonlinear effects are crucial;
- once the perturbation wave number become sub–Planckian we can trust the standard linear evolution. Yet, this evolution will keep the memory of the initial condition at the matching point given by $k/a = \Lambda$
- at energies larger than Λ fluctuations may give rise to trapped surfaces, which is to say they can produce a black hole environment. As gravitational interactions are nonlinear, tensor fluctuations with a high k will interact with this environment so that the evolution can be effectively described in terms of a non-homogeneous differential equation with a source term.

4.2 Tensor perturbation evolution

Given these points, the model proposed is the following. We introduce a non-vanishing anisotropic stress tensor that will encode information about the chaotic environment from which each mode has to go through when it starts evolving. We generalize equation 3.83, by adding a source term acting on modes inside the horizon satisfying the condition $k/a > \Lambda$, or $\eta < \bar{\eta}_k$. This translates into a two-stage evolution:

$$h_k'' + 2\mathcal{H}h_k' + k^2 h_k = 16\pi G a^2 \Pi_k \qquad \eta < \bar{\eta}_k \tag{4.1}$$

$$h_k'' + 2\mathcal{H}h_k' + k^2 h_k = 0 \qquad \eta > \bar{\eta}_k \tag{4.2}$$

with the matching conditions:

$$\begin{aligned} \lim_{\eta \to \bar{\eta}_k^-} h_k(\eta) &= \lim_{\eta \to \bar{\eta}_k^+} h_k(\eta) \\ \lim_{\eta \to \bar{\eta}_k^-} h_k'(\eta) &= \lim_{\eta \to \bar{\eta}_k^+} h_k'(\eta) \end{aligned} \tag{4.3}$$

An initial condition can be imposed, as in the Bunch-Davies case, so that for $\eta \to -\infty$ the fluctuation has the lowest energy allowed by the uncertainty principle.

Differently than the approach described in section 3.2.5, here $\bar{\eta}_k$ is the time where the source term switches off and the evolution of the (now sub–Planckian) mode is the usual one. Π_k is supposed to be a stochastic incoherent source that satisfies the conditions of the Brownian motion:

$$\begin{aligned} \langle \Pi_k(\eta) \rangle &= 0 \\ \langle \Pi_k(\eta)\Pi_k^*(\eta') \rangle &= \Lambda^6 \delta(\eta-\eta') \left| F\left(\frac{k}{a\Lambda}, \frac{\Lambda}{M_{\mathrm{Pl}}}\right)\right|^2 \end{aligned} \tag{4.4}$$

where $\langle \dots \rangle$ denotes average over the probability function. The prefactor has been placed to comply with the dimensionality of Π_k while F takes into account the dependence of the source on k and the relative value of Λ with respect to the Planck mass. The shear source has to be quantized as with metric fluctuations:

$$\hat{\Pi}^r_{\mathbf{k}}(\eta) = \Pi_k(\eta)\hat{a}^r_{\mathbf{k}} + \Pi_k^*(\eta)\hat{a}^{r\dagger}_{-\mathbf{k}} \tag{4.5}$$

Equation 4.2 has solution:

$$h_k(\eta) = \frac{A_k}{a(\eta)} \frac{e^{-ik\eta}}{\sqrt{2k}}\left(1 - \frac{i}{k\eta}\right) + \frac{B_k}{a(\eta)}\frac{e^{ik\eta}}{\sqrt{2k}}\left(1 + \frac{i}{k\eta}\right) \tag{4.6}$$

while equation 4.1 has solution:

$$h_k(\eta) = \frac{16\pi G}{a(\eta)} \int_{-\infty}^{\eta} d\eta' a(\eta') G_k(\eta,\eta')\Pi_k(\eta') \tag{4.7}$$

in terms of the Green function:

$$\begin{aligned} G_k(\eta,\eta') = \frac{e^{-ik(\eta+\eta')}}{2k^3\eta'^2} \Big[& e^{2ik\eta}(1-ik\eta)(-i+k\eta') \\ & +e^{2ik\eta'}(1+ik\eta)(i+k\eta')\Big] \Theta(\eta-\eta') \end{aligned} \tag{4.8}$$

Using the matching conditions 4.3, and making the average as in the Langevin approach to Brownian motion, the coefficients A_k and B_k are calculated:

$$\begin{aligned} \frac{A_k}{a\left(\bar{\eta}_k\right)} &= e^{ik\bar{\eta}_k}\left[h\left(\bar{\eta}_k\right)\left(-1+ik\bar{\eta}_k+k^2\bar{\eta}_k^2\right)\right. \\ &\quad \left. -h_k'\left(\bar{\eta}_k\right)\left(\bar{\eta}_k - ik\bar{\eta}_k^2\right)\right]\left(\sqrt{2}k^{3/2}\bar{\eta}_k^2\right)^{-1} \\ \frac{B_k}{a\left(\bar{\eta}_k\right)} &= e^{-ik\bar{\eta}_k}\left[h\left(\bar{\eta}_k\right)\left(-1-ik\bar{\eta}_k+k^2\bar{\eta}_k^2\right)\right. \\ &\quad \left. -h_k'\left(\bar{\eta}_k\right)\left(\bar{\eta}_k + ik\bar{\eta}_k^2\right)\right]\left(\sqrt{2}k^{3/2}\bar{\eta}_k^2\right)^{-1} \end{aligned} \tag{4.9}$$

From 4.6 we see that $h_k \sim k^{-1/2}$, therefore these coefficient depend on the adimensional quantity $k\bar{\eta}_k = -\Lambda/H$, so that the predicted power spectrum is still scale invariant:

$$\mathcal{P}_h(k) = \mathcal{P}_h^{\mathrm{BD}}(k)\left[1 + \left|B_k\right|^2 \left(2 + \frac{2k\bar{\eta}_k + i}{i}e^{2ik\bar{\eta}_k} - \frac{2k\bar{\eta}_k - i}{i}e^{-2ik\bar{\eta}_k}\right)\right] \tag{4.10}$$

where $\mathcal{P}_h^{\mathrm{BD}}$ is the standard power spectrum from BD vacuum.

4.3 The shear source model

The authors of the paper [4] also propose a model to describe the source term in 4.1 by the specification of the adimensional function F. The scenario is named the "BH gas" model.

As mentioned before, in the trans-Planckian regime, modes with $k > a\Lambda$ experience quantum gravity effects, which determine the interaction of the fluctuations with the background. This means that perturbations form an **open system**. The background can be effectively described as a black hole gas which is formed when trapped surfaces create. The gas produces particles, in particular gravitational wave, through Hawking radiation, which act as a source for $h(\eta)$. Given a probability distribution of the BH's as a function of their mass M, $\xi(M)$, and approximating the Hawking emission spectrum with a Boltzmann shape we have

$$F\left(\frac{k}{a\Lambda}, \frac{\Lambda}{M_{\mathrm{Pl}}}\right) = \int_0^\infty \xi(M)\exp\left(-\frac{k}{a}\frac{8\pi M}{M_{\mathrm{Pl}}^2}\right)dM \tag{4.11}$$

The parameter Λ represents, in terms of the distribution $\xi(M)$, a natural cut-off scale for the black hole mass distribution. Using a simple form for $\xi(M)$:

$$\xi(M)dM = \frac{1}{\Lambda}e^{-M/\Lambda}dM \tag{4.12}$$

the result is

$$F\left(\frac{k}{a\Lambda}, \frac{\Lambda}{M_{\mathrm{Pl}}}\right) = \left(1 + \frac{k}{a\Lambda}\frac{8\pi\Lambda^2}{M_{\mathrm{Pl}}^2}\right)^{-1} \tag{4.13}$$

4.4 Results

Authors have numerically solved equations 4.1 and 4.2 with 4.13. The most remarkable feature of this model is that it still predicts a scale invariant spectrum. Figure 4.1 show the ratio $\mathcal{P}_h/\mathcal{P}_h^{\mathrm{BD}}$ as function of the ratio Λ/M_{Pl}.

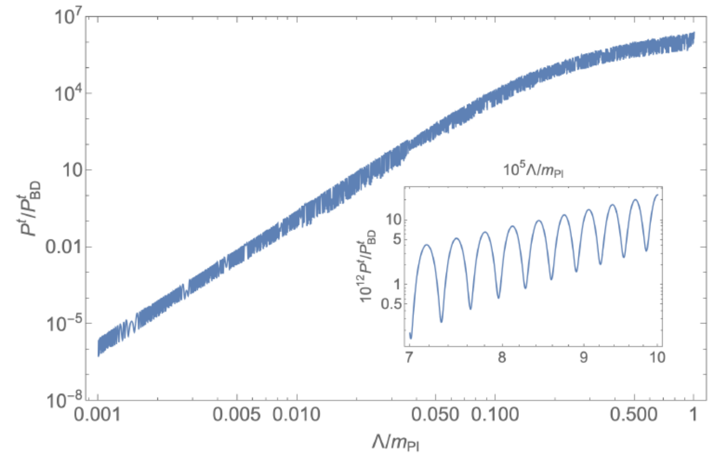

Figure 4.1: *The obtained power spectrum (here called P^t) normalized to the standard BD spectrum versus the ratio Λ/M_{Pl}. A zoom-in plot is provided for a smaller range of the ratio Λ/M_{Pl}.*

Two features are worth to be underlined: a very rapid oscillatory behaviour of the ratio and its wide span (from 10^{-6} to 10^{6}) in the Λ definition range. The former feature is due of the trigonometric dependence of $\mathcal{P}_h$ on Λ while the latter is due to the interference term in 4.10 and to the source scale Λ^3 which weights its amplitude.

The value of Λ for which the predicted spectrum is of the same order than the standard $\mathcal{P}_h^{\mathrm{BD}}$ is roughly $10^{-2}M_{\mathrm{Pl}}$.

4.5 Outlooks

This research has revealed that introducing a stochastic source term in the evolution of tensor perturbations with energy above a cut-off scale Λ produces a scale invariant tensor power spectrum with an amplitude that agrees with the BD result for $\Lambda \sim 10^{-2}M_{\mathrm{Pl}}$. This approach can be in principle also extended to scalar perturbations, with similar results. Scalar perturbations however are more sensitive to the details of the considered inflationary model, while tensor modes only depend upon initial conditions, possible quantum effects and the value of the almost constant Hubble scale during inflation. At first glance, scalar perturbations should experience the same behaviour in the trans-Planckian regime described here. Therefore we expect the tensor to scalar ratio to be independent from Λ.

In addition to that, recall that in the standard case scalar perturbations amplitude depends only on the Hubble parameter and the features of the inflaton potential (i.e. the slow-roll parameter). Adding the parameter Λ in the dynamics of fluctuations in the high energy regime may provide different results for what we know about the inflation dynamics, as we expect

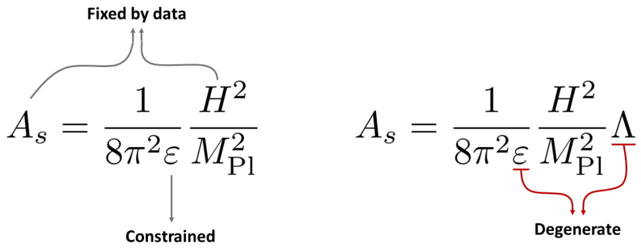

Figure 4.2: *The degeneracy induced by Λ*

some extra degeneracies among the slow-roll parameters and Λ, once the perturbation amplitude at large CMB scale is fixed by data.

4.6 The main idea

All the above considerations lead us to the idea that lies at the basis of this thesis work. Numerous models for inflation dynamics are currently ruled out because of the constraints on the slow roll parameter ε imposed by the CMB data on the standard BD model. What if ε can have some extra degrees of freedom?
Performing a likelihood analysis of primordial spectrum parameters (including the feature Λ) can return new allowed values for the slow-roll parameter, opening the path for new inflationary models and providing us with some vital information about the inflation dynamics (i.e. the inflaton potential). Figure 4.2 highlights the extra degeneracy induced by the addition of Λ in the primordial spectrum.

In the following chapters, all details will be presented about the mathematical and technical tools needed to perform this likelihood analysis.

CHAPTER

5

BAYESIAN METHODS

All scientific questions in cutting-edge research involve increasingly complex models aimed at explaining subtle effects observed through complex and highly multidimensional datasets. Consequently, statistical tools must keep pace with the growing complexity of the analyses to be performed. Statistical inference is a fundamental part of research as it allows for the analysis and interpretation of data, as well as the verification and comparison of models, while simultaneously providing estimates for their parameters. Bayesian statistics offers an approach to parameter estimation based on Bayes' theorem. In the following sections, the conceptual, analytical, and numerical elements necessary to tackle the most common inference problems in cosmology and physics in general will be provided.

5.1 Basic Notions

Let $A, B, C, \ldots$ denote propositions and let Ω denote the sample space. The **probability** (in the classical "frequentist" approach) of an event is the number of times it occurs divided by the total number of possible events in the limit of an infinite series of equiprobable trials. This definition has the advantage of being an operational definition, thus providing a method for calculation. However, it presents the following problematic aspects:

- from a formal standpoint, it is a circular definition, as it requires that cases have equal probability, which is precisely what it aims to define;
- it does not define probability in the case of non-equiprobable events;
- in many situations, it is rather presumptuous to assume that one can know all possible cases (e.g., all theories that could explain a particular phenomenon, in order to calculate which is the most probable).

The Bayesian outlook is that probability expresses a degree of belief in a proposition, based on the available knowledge of the experimenter. First of all, two essential quantities are defined in the following way.

The **joint probability** of A and B is the probability of A and B happening together, and is denoted by $P(A, B)$.

The **conditional probability** of A given B is the probability of A happening given that B has happened, and is denoted by $P(A|B)$.
They obey the product rule

$$P(A, B) = P(A|B)P(B) \tag{5.1}$$

Inverting A and B:

$$P(B, A) = P(B|A)P(A) \tag{5.2}$$

and, because $P(A, B) = P(B, A)$, we obtain the **Bayes theorem**:

$$P(A|B) = \frac{P(B|A)P(A)}{P(B)} \tag{5.3}$$

5.2 Inference and likelihood

The problem of inference concerns establishing the properties of the probability distribution underlying a statistical process, given a collection of samples $\{\hat{x}_1, \hat{x}_2, \ldots, \hat{x}_N\}$.

Given a random variable X with its probability density function (pdf) $p(X|\theta)$, where θ is a collection of parameters, and a dataset $\hat{x} = \{\hat{x}_1, \hat{x}_2, \ldots, \hat{x}_N\}$, the likelihood function $\mathscr{L}$ is defined as

$$\mathscr{L}(\theta) = P(\hat{x}|\theta) \tag{5.4}$$

namely, the probability of observing the data that have been obtained as a function of the parameters θ. Note that the likelihood is *not* a pdf in θ. In the search for the best values of θ, the best choice should therefore be the one that maximises the likelihood, as this maximises the probability of obtaining the taken data. Notice that this is not necessarily the same as maximising the probability of θ. As will be seen, doing so requires the use of Bayes theorem. This choice is known as the **maximum likelihood principle**:

$$\theta_{\mathrm{ML}} \equiv \max_{\theta} \mathscr{L}(\theta) \tag{5.5}$$

The conventional procedure to find the maximum consists in the requirement that the first derivative of the logarithm of the likelihood vanishes and that its second derivative is negative:

$$\left.\frac{\partial \ln \mathscr{L}(\theta)}{\partial \theta}\right|_{\theta_{\mathrm{ML}}} = 0 \qquad \left.\frac{\partial^2 \ln \mathscr{L}(\theta)}{\partial \theta^2}\right|_{\theta_{\mathrm{ML}}} < 0 \tag{5.6}$$

5.3 Bayesian inference

In this section the Bayesian approach to the probability will be introduced. This simple application of the Bayes theorem encapsulates the notion of probability as degree of belief.

5.3.1 Bayes theorem

As a mathematical result, Bayes Theorem is elementary and uncontroversial. It becomes interesting for the purpose of inference when we replace in Bayes theorem, equation 5.3 , $A \to \theta$ (the parameters) and $B \to d$ (the observed data, or samples), obtaining:

$$P(\theta|d) = \frac{P(d|\theta)P(\theta)}{P(d)} \tag{5.7}$$

On the left hand side, $P(\theta|d)$ is the posterior probability for θ and it represents our degree of belief about the value of θ after we have seen the data d.

On the right hand side, $P(d|\theta) = \mathscr{L}(\theta)$ is the likelihood we already encountered. It is the probability of the data given a certain value of the parameters.

The quantity $P(\theta)$ is the prior probability distribution. It represents our degree of belief in the value of θ before we see the data. The choice of the prior is at the researcher's discretion. We will discuss about this later. Eventually, however formulated is the prior, the posterior distribution usually converges to a prior-independent regime for sufficiently large data sets.

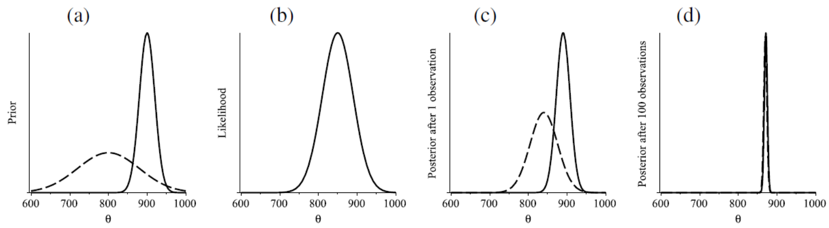

Figure 5.1: *Converging views in Bayesian inference. Image taken from reference [12]*

In the denominator, $P(d)$ is a normalizing constant, called **Bayesian evidence** or "marginal likelihood", than ensures that the posterior is normalized to unity:

$$P(d) = \int d\theta P(d|\theta)P(\theta) \tag{5.8}$$

Bayesian inference works by updating our state of knowledge about a parameter (or hypothesis) as new data flow in. The posterior from a previous cycle of observations becomes the prior for the next.

5.3.2 Choice of the prior

Bayesian inference requires the specification of an initial prior, which is not determined by the theory, but needs to be given by the user. The prior should represent fairly the state of knowledge of the user about the quantity of interest. Eventually, the posterior will converge to a unique (objective) result even if different scientists start from different priors (provided their priors are non-zero in regions of parameter space where the likelihood is large, see image 5.1).

In many situations prior information is highly relevant and omitting it would result in seriously wrong inferences. The simplest case is when the parameters of interest have a physical meaning that restricts their possible values: masses, count rates, power and light intensity are examples of quantities that must be positive. There is a vast literature about how to select a prior in an appropriate way. Some aspects are fairly obvious: if your parameter θ describes a quantity that has to be strictly positive (such as the number of photons in a detector, or an amplitude), then the prior will be 0 for values $\theta < 0$.

A very common choice is the "flat prior":

$$P(\theta) = \begin{cases} \frac{1}{(\theta_{\max}-\theta_{\min})} & \theta_{\min} \leq \theta \leq \theta_{\max} \\ 0 & \text{otherwise} \end{cases} \tag{5.9}$$

It expresses the minimum knowledge about the parameter. For a Gaussian likelihood it has, in fact, the maximum entropy for the mean parameter.

5.3.3 Model selection

In the most common case, Bayesian inference is used when a chosen model $\mathscr{M}_0$ is assumed true and we want to learn about its parameters θ_0. Sometimes, one has also a series of alternative models ($\mathscr{M}_1, \mathscr{M}_2, \ldots$) and wants to determine which one is in best agreement with the data. In case there is no clear best model, one can still make inferences on parameters that account for this model uncertainty.The frequentist approach to model criticism is in the form of hypothesis testing. One ends up rejecting (or not) a null hypothesis H_0 based on the p-value, i.e., the probability of getting data as extreme or more extreme than what has been observed if one assumes that H_0 is true. Notice that this is *not* the probability for the hypothesis! Classical hypothesis testing assumes the hypothesis to be true and determines how unlikely are our observations given this assumption. One might be interested in the probability of the hypothesis itself given the observations in hand.

The Bayesian approach does not reject a model unless there are specific alternatives available: it takes therefore the form of model comparison. The key quantity for model comparison is the Bayesian evidence. Bayesian model comparison automatically implements a quantitative version of Occam's razor, namely, the notion that simpler models ought to be preferred if they can explain the data sufficiently well.

Recalling the Bayesian evidence from equation 5.7, conditioning explicitly on the model under consideration $\mathscr{M}$ with parameter space $\Omega_{\mathscr{M}}$:

$$p(d|\mathscr{M}) \equiv \int_{\Omega_{\mathscr{M}}} p(d|\theta, \mathscr{M}) p(\theta|\mathscr{M}) d\theta \tag{5.10}$$

the model posterior probability given the data is obtained by using Bayes theorem to invert the order of conditioning:

$$p(\mathscr{M}|d) \propto p(\mathscr{M}) p(d|\mathscr{M}) \tag{5.11}$$

When comparing two models $\mathscr{M}_0$ and $\mathscr{M}_1$, the quantity of interest is the ratio of the posterior probabilities, given by:

$$\frac{p(\mathscr{M}_0|d)}{p(\mathscr{M}_1|d)} = B_{01} \frac{p(\mathscr{M}_0)}{p(\mathscr{M}_1)} \tag{5.12}$$

where

$$B_{01} \equiv \frac{p(d|\mathscr{M}_0)}{p(d|\mathscr{M}_1)} \tag{5.13}$$

is called **Bayes factor**. A value $B_{01} > (<)\, 1$ represents an increase (decrease) of the support in favour of model 0 versus model 1 given the observed data.

5.4 Numerical applications

In this section I will introduce the most widely used algorithms constructed with the task of calculating the quantities of greatest interest in Bayesian statistics, i.e. the posterior distribution and the Bayesian evidence.

5.4.1 Markov chain Monte Carlo (MCMC)

General theory

The purpose of a Markov chain Monte Carlo algorithm is to construct a sequence of points in parameter space, called a chain. The crucial property of the chain is that the density of samples is proportional to the posterior pdf. This allows to construct a map of the posterior distribution.

A chain is defined as a sequence of random points $\{\theta^{(0)}, \theta^{(1)}, \ldots, \theta^{(M)}\}$ such that the probability of the $(t+1)$-th element in the chain only depends on the value of the t-th element. It is possible to show [12] that a chain converges to a stationary point. The generation of the elements of a chain is governed by a *transition probability* $T(\theta^{(t)}, \theta^{(t+1)})$ that satisfies the detailed balance condition:

$$p(\theta^{(t)}|d)T(\theta^{(t)}, \theta^{(t+1)}) = p(\theta^{(t+1)}|d)T(\theta^{(t+1)}, \theta^{(t)}) \tag{5.14}$$

Once the chain has converged and the points have been gathered, any expectation value can be calculated with the following approximation:

$$E[f(\theta)] = \int P(\theta|d)f(\theta)d\theta \approx \frac{1}{M}\sum_{t=0}^{M} f(\theta^{(t)}) \tag{5.15}$$

It is often interesting to provide the **marginal posterior** for each of the parameters θ_j:

$$P(\theta_j|d) = \int P(\theta|d)d\theta_1 \ldots d\theta_{j-1}d\theta_{j+1}\ldots d\theta_n \tag{5.16}$$

This integration can be numerically complicated, but since the density of the MCMC points reflects the full posterior $P(\theta|d)$, it is sufficient to divide the range of θ_j in bins and count the number of points in each bin, simply ignoring all other parameters.

The Metropolis-Hastings algorithm

The most used algorithm for MCMC computation is the following **Metropolis-Hastings** algorithm:

1. Start from a random point $\theta^{(0)}$, with associated posterior probability $p_0 \equiv (\theta^{(0)}|d)$;

2. Propose a candidate point $\theta^{(c)}$ by drawing from a proposal distribution $q(\theta^{(0)}, \theta^{(c)})$;

3. Evaluate the posterior at the candidate point, $p_c = p(\theta^{(c)}|d)$ and accept the candidate point with probability

$$\alpha = \min\left(\frac{p_c q(\theta^{(c)}, \theta^{(0)})}{p_0 q(\theta^{(0)}, \theta^{(c)})}, 1\right) \tag{5.17}$$

   (this can be performed by generating a random number u from the uniform distribution $[0, 1)$ and accepting the candidate sample if $u < a$ and rejecting it otherwise);

4. If the candidate point is accepted, add it to the chain and move there. Otherwise stay at the old point (which is thus counted twice in the chain). Go back to point 2.

For the Metropolis algorithm, the distribution q satisfies the symmetry condition $q(x, y) = q(y, x)$ and the quantity α simplifies to

$$\alpha = \min\left(\frac{p_c}{p_0}, 1\right) \tag{5.18}$$

It can be shown that the Metropolis algorithm satisfies the detailed balance condition 5.14, with the transition probability given by

$$T(\theta^{(t)}, \theta^{(t+1)}) = q(\theta^{(t)}, \theta^{(t+1)})\alpha(\theta^{(t)}, \theta^{(t+1)}) \tag{5.19}$$

The choice of proposal distribution q is crucial for the efficient exploration of the posterior. If the scale of q is too small compared to the scale of the target distribution, exploration will be poor as the algorithm spends too much time locally. If instead the scale of q is too large, the chain gets stuck as it does not jump very frequently.

5.4.2 Nested sampling

An alternative to classical MCMC methods is the so-called "nested sampling" algorithm. Although the original motivation for nested sampling was to compute the evidence integral of equation 5.10, the development of the multi–modal nested sampling technique provides a powerful and versatile algorithm that can sample efficiently from complex, multi-modal likelihood surfaces [12].

The idea is to recast the multi–dimensional evidence integral into a one–dimensional integral, by defining the prior volume:

$$X(\lambda) = \int_{\mathscr{L}(\theta)>\lambda} p(\theta|\mathscr{M})d\theta \tag{5.20}$$

where $\mathscr{L}(\theta) \equiv p(d|\theta, \mathscr{M})$. Therefore $X(\lambda)$ gives the volume of parameter space above a certain level λ of the likelihood. The Bayesian evidence can be written as

$$p(d|\mathscr{M}) = \int_0^1 \mathscr{L}(X)dX \tag{5.21}$$

where $\mathscr{L}(X)$ is the inverse of equation 5.20. Samples from $\mathscr{L}(X)$ can be obtained by drawing uniformly samples from the likelihood volume defined by λ. Finally, the 1–dimensional integral of equation 5.21 can be obtained in the following approximation:

$$p(d|\mathscr{M}) \approx \sum_i \mathscr{L}(X_i)W_i \tag{5.22}$$

where $W_i \equiv \frac{1}{2}(X_{i-1} - X_{i+1})$.

Nested Sampling procedure

Here is a simple version of the nested sampling algorithm [10]:

1. Start with N points $\theta_1, \ldots, \theta_N$;
   Initialize $Z = 0$ and $X_0 = 1$
   For $i = 1, \ldots, j$ do the following:
   (a) Record the lowest of the current likelihood values as L_i,
       Set $Xi = \exp(-i/N)$ or sample it to get uncertainty,
       Set $w_i = X_{i-1} - X_i$,
       Increment Z by $L_i w_i$,

   (b) Update the point with least likelihood with some Markov chain Monte Carlo steps according to the prior, accepting only steps that keep the likelihood above L_i.

At each iteration, X_i is an estimate of the amount of prior mass covered by the volume in parameter space of all points with likelihood greater than

θ_i. The weight factor w_i is an estimate of the amount of prior mass that lies between two surfaces $p(d|\theta_{i-1}, \mathscr{M})$ and $p(d|\theta_i, \mathscr{M})$. The update step $Z := Z + L_i w_i$ computes the sum over i of $L_i w_i$ to numerically approximate the integral $p(d|\mathscr{M})$.

Termination of the main loop could simply be after a preset number of steps, or could be when even the largest current likelihood, taken over the full current box, would not increase the current evidence by more than some small fraction f.

5.5 The codes

In this section, I will present the numerical and statistical analysis codes used to achieve the goals of this thesis work. The first code, CAMB, is a numerical analysis tool that solves the complex system of equations governing the evolution of the universe and each of its main components across all epochs. Following this, the Cobaya code, a Bayesian analysis tool specialized for cosmology, is introduced. Cobaya includes implementations of MCMC (Markov Chain Monte Carlo) and a specific nested sampling algorithm called PolyChord, which allow for the estimation of posterior distributions for all the parameters of a model, given some preliminary input information.

5.5.1 CAMB

CAMB (Code for Anisotropies in the Microwave Background) is a numerical code designed to compute theoretical predictions for cosmological observables, particularly the Cosmic Microwave Background (CMB) anisotropies, matter power spectra, and other related quantities. The primary purpose of CAMB is to solve the Einstein-Boltzmann equations that govern the evolution of perturbations in the universe, considering the contributions from various components such as dark matter, baryons, photons, neutrinos, and dark energy.

CAMB takes as input a set of cosmological parameters, including the Hubble constant, matter density, dark energy density, curvature, primordial power spectrum parameters, and reionization history, among others. Additionally, it requires initial conditions for the perturbations, typically provided by models of inflation.

The code operates by first solving the background evolution of the universe, followed by the computation of linear perturbations using the Einstein-Boltzmann equations. These equations are integrated across different scales and redshifts to produce power spectra for the CMB temperature and polarization, as well as the matter power spectrum. CAMB can also account for various effects such as lensing, non-standard recombination histories, and neutrino masses. The results from CAMB are widely used in cosmological parameter estimation, enabling researchers to compare theoretical predictions with observational data.

The code is structured into modules, each of which considers a specific model for different cosmological phases (e.g., BBN, reionization, etc.) and components of the universe (e.g., dark matter, baryons, etc.). The parameters required for the execution of each of these modules are listed and specified in an additional file specifically for the initialization of these parameters. For the purpose of this thesis, the only module that required modification is the one dedicated to the primordial power spectrum, "`InitialPower.f90`". The advantage of this modularity is that, in the case of the `InitialPower` module, all parameters are defined and evaluated within the module itself, making it unnecessary to modify other parts of the code. The original code implements a power spectrum described by the function 3.81. Modifications to this function and the introduction of new parameters can impact predictions for cosmological observables such as the CMB spectrum or matter power spectra.

As an example, two different choices for the primordial spectrum will be presented here (figure 5.2): one is the standard scale-invariant spectrum defined in equation 3.81, while the other is a modification of the first, consisting of the addition of an oscillatory feature:

$$\mathcal{P}(k) = \left[1 + Ae^{-\frac{1}{\mu}\frac{k}{k_0}} \sin\left(\nu \frac{k}{k_0}\right)\right] \mathcal{P}_{\text{std}}(k) \tag{5.23}$$

where $P_{\text{std}}(k)$ is the spectrum 3.81 and $A = 2$, $\mu = 0.5$ and $\nu = -10$.

5.5.2 Cobaya

Cobaya is a sophisticated Bayesian inference framework designed specifically for cosmological analyses. Its primary purpose is to estimate the posterior distributions of cosmological parameters by comparing theoretical models to observational data. Cobaya is built to handle complex, high-dimensional parameter spaces, making it an essential tool for modern cosmology, particularly in analyzing data from the Cosmic Microwave Background (CMB), large-scale structure, and other cosmological probes.

Cobaya operates by implementing Markov Chain Monte Carlo (MCMC) methods and nested sampling techniques, with a notable integration of the PolyChord algorithm for efficient sampling in high-dimensional spaces. The

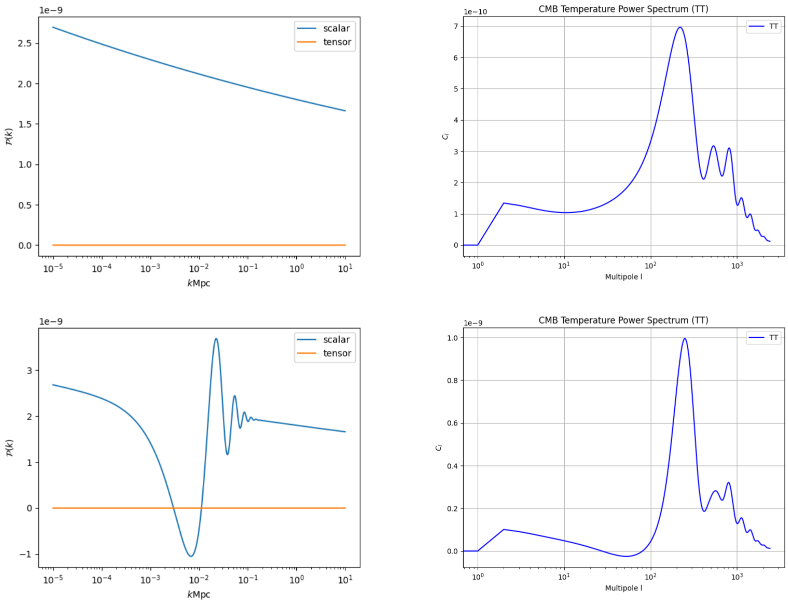

Figure 5.2: *Two different choices for the initial power spectrum produce different CMB spectra after CAMB evaluation. Notice that the oscillatory spectrum determines a lower power at low multipoles.*

code is highly modular, allowing users to define cosmological models, likelihoods, and priors in a flexible manner.

The input to Cobaya typically includes the cosmological parameters to be estimated, their prior distributions, the theoretical models (often implemented through CAMB or CLASS), and the likelihood functions corresponding to the observational datasets. Additionally, users can specify settings related to the MCMC chains, convergence criteria, and output formats.

Cobaya's mechanism involves generating a large number of samples from the posterior distribution by iteratively refining the parameter space based on the likelihood of the models given the data. The output consists of posterior distributions, evidence values, and other statistical summaries, which are then used to constrain cosmological models and derive conclusions about the underlying physics of the universe.

For each particular run, the input must describe the model and its parameter space in enough detail, and also specify the analysis tool that will be used. Cobaya's input takes the form of a Python dictionary, and can be serialized in plain text in the YAML format.

The Bayesian Model consists of the Bayesian prior and likelihood (this last one including theory and experimental likelihood components). It also contains a parameterization layer that manages the flow of parameters to and from the likelihood and prior, and computes the dynamically-defined ones, and a provider that handles the exchange of parameters and computed quantities between different theory and likelihood components. A model

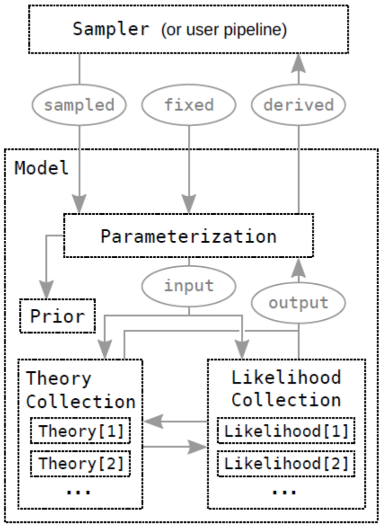

Figure 5.3: *Simplified structure of Cobaya's source, showing classes (squares) and parameters (ellipses).*

instance can be passed as an argument to a sampler, or it can be integrated by the user into an external pipeline.

On their way out of the model, parameters can play three different roles:

- *Sampled* parameters are the ones whose value is to be varied and explored by the sampler or the user defined pipeline. They are identified in the input by having a defined prior;
- *Fixed* parameters are those whose value is not going to change, and are needed as input by some piece of the Model.
- *Derived* parameters are arbitrary functions of the rest of the parameters at every step, and are tracked and stored for the user's convenience. Functions defining them can be provided in the input file or can be implicitly defined inside the code of a theory or likelihood.

The parameterization class processes the parameters to turn them into input parameters for the likelihoods and theories, and requests from them the output parameters that are needed to compute derived parameters that cannot be computed directly from inputs. The parameterization layer also manages other properties of the parameters, such as their labels (used for plots). [11] Figure 5.3 gives a representation of this working mechanism.

Monte Carlo samplers in Cobaya take models and explore their sampled parameters. Cobaya implements adaptive MCMC samplers [8], that include a Metropolis-Hastings MCMC algorithm. In addition, it contains a wrapper for the nested sampler PolyChord [5] [6], which can also estimate model evidences and explore complicated multi-modal likelihood surfaces.

At the end of its operation, Cobaya writes the samples to the hard drive, storing them in plain text as parameter tables, including the corresponding probabilities and sample weights. Both the sample objects and output files can be easily loaded and analysed with the user's tool of choice. The suggested analysis package is GetDist4 [7], which can load Cobaya results transparently. GetDist provides summary statistics including confidence intervals, density estimates (via optimized kernel density estimation), and convergence diagnostics, plotting tools, and a graphical user interface.

As an example, I will present an analysis conducted on cosmological parameters defined within an inflationary model that includes a generic oscillatory feature given by

$$\mathcal{P}(k) = \left[1 + Ae^{-\frac{1}{2}\left[\frac{\log_{10}\left(\frac{k}{k_c}\right)}{w}\right]^2} \sin\left(2\pi\frac{k}{l}\right)\right]\mathcal{P}_{\mathrm{std}}(k) \tag{5.24}$$

where $P_{\mathrm{std}}(k)$ is again the standard spectrum 3.81 and (A, k_c, w, l) are the new parameters introduced by this inflationary scenario. In this analysis, the theory provided to Cobaya is based on the CAMB code, excluding the `InitPower.f90` module, and defining the primordial spectrum 5.24 within an external Python script. The data used are from the Planck 2018 collaboration [1], and the chosen priors for the parameters were all flat. The sampler utilized was PolyChord. Figure 5.4 shows the YAML file provided as input to Cobaya, while figure 5.5 presents a plot of the marginalized posterior distributions over one and two parameters.

```
theory:
  theory_primordial_Pk.FeaturePrimordialPk:
    python_path: .
    k_pivot: 0.05
    n_samples_wavelength: 20
  camb:
    external_primordial_pk: true
    extra_args: {lens_potential_accuracy: 5, Accuracy.IntkAccuracyBoost: 1, Accuracy.lSampleBoost: 3,
halofit_version: mead, bbn_predictor: PArthENoPE_880.2_standard.dat, num_massive_neutrinos: 1, nnu:
3.046, theta_H0_range:[20,100]}
likelihood:
  planck_2018_lowl.TT: null
  planck_2018_lowl.EE: null
  planck_2018_highl_plik.TTTEEE: null
  planck_2018_lensing.clik: null

params:
  logamplitude:
    prior: [-2,-0.6]
    ref: {dist: norm, loc: -1.1, scale: 0.05}
    proposal: 0.2
    latex: \log_{10}A_\mathrm{feature}
  amplitude:
    value: ’lambda logamplitude: 10**logamplitude’
    latex: A_\mathrm{feature}
  logwavelength:
    prior: [-2.5,-1.8]
    ref: {dist: norm, loc: -2.1, scale: 0.001}
    proposal: 0.0005
    latex: \log_{10}l_\mathrm{feature}
  wavelength:
    value: ’lambda logwavelength: 10**logwavelength’
    latex: l_\mathrm{feature}
  logcentre:
    prior: [-1.15,-0.3]
    ref: {dist: norm, loc: -0.7, scale: 0.008}
    proposal: 0.1
    latex: \log_{10}k_{c,\mathrm{feature}}
  centre:
    value: ’lambda logcentre: 10**logcentre’
    latex: k_{c,\mathrm{feature}}
  logwidth:
    prior: [0.001,3]
    ref: {dist: norm, loc: 0.1, scale: 0.02}
    proposal: 0.05
    latex: w_\mathrm{feature}

sampler:
  polychord:
    nlive: d
    num_repeats: d
    precision_criterion: 0.001
output: delensed
timing: true
```

Figure 5.4: *Cobaya’s input in YAML format for the use case described in this section. Baseline ΛCDM cosmological parameters definitions (prior, reference pdf, etc.) are omitted here for brevity.*

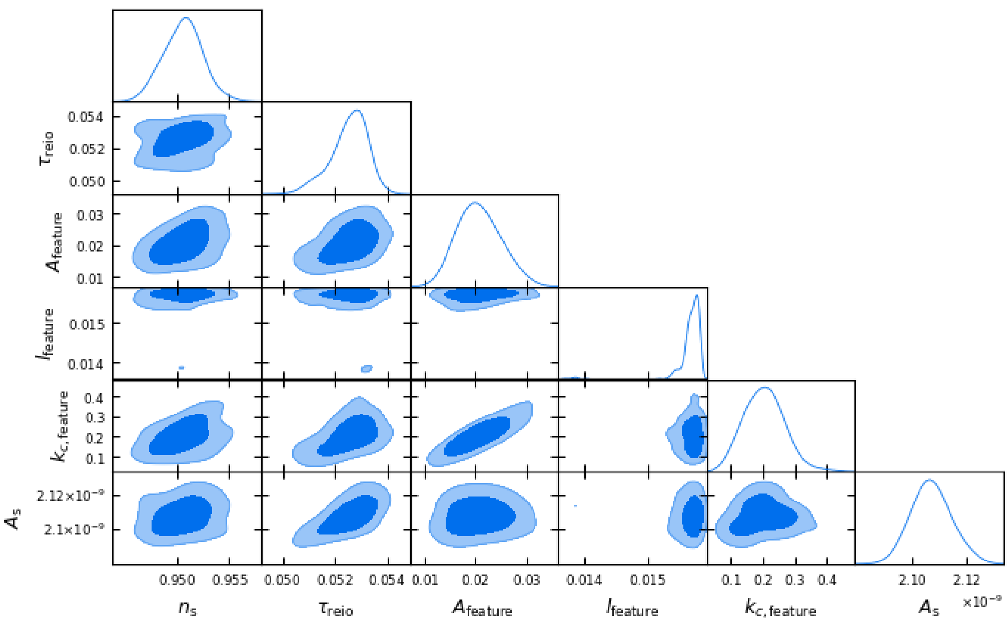

Figure 5.5: *1- and 2-d marginalized posteriors for the feature parameters in the use case described in this section.*

CHAPTER

6

STOCHASTIC MODEL PARAMETER ANALYSIS

Physics is about taking seriously a universe
that is merely playing tricks on us.

Having presented the analytical and technical tools necessary for performing the likelihood analysis of the parameters, I will now outline the steps followed in conducting this analysis, as previously mentioned in section 4.6. The primary challenge anticipated in approaching this type of problem lies in the potential degeneracy of the parameters. In the current literature, there are few studies that have utilized Bayesian analysis software on systems with highly degenerate parameters. Moreover, the possible degeneracy of the inflationary parameters is a key focus of this thesis, as it could potentially open up broader possibilities for modeling the inflaton scalar field, particularly its potential. Given the novelty and technical difficulties associated with this issue, the analysis was carried out through gradual advancements. Specifically, two main intermediate steps were undertaken: first, an analysis of the inflationary parameters was conducted by decomposing the amplitude A_s of the primordial perturbation spectrum into the Hubble parameter and the slow-roll parameter as described in equation 3.79; subsequently, the analysis was repeated with the addition of the parameter Λ as described in figure

4.6, using the data obtained from the previous analysis to inform the priors for the subsequent one. I will now proceed to describe these two steps in more detail. The data used for the subsequent analyses were obtained from the Planck 2018 survey [1] and employed the full set of spectra (TT, TE, EE, and lensing).

6.1 Preliminary amplitude decomposition

Since the amplitude of scalar perturbations is a cosmological parameter directly measurable through CMB observations, it is analyzed individually, without being decomposed into the Hubble and slow-roll parameters as per equation 3.79. These two parameters are subsequently determined through successive iterations. In an effort to alleviate the constraints imposed on the value of ϵ, the initial part of the study focused on analyzing the inflationary parameters by substituting the amplitude in expression 3.81 with its functional dependence given by equation 3.79, treating the two parameters H and ϵ as independent. This approach is theoretically feasible because, during inflation, these two quantities remain nearly constant and can be effectively treated as parameters. The analysis proceeded by inputting the CAMB code into Cobaya, excluding the `InitPower.f90` module, and providing the following expression

$$\mathcal{P}(k) = \frac{1}{8\pi^2\varepsilon}\frac{H^2}{M_{\rm Pl}^2}\left(\frac{k}{k_*}\right)^{n_s-1} \tag{6.1}$$

as the primordial spectrum. The sampler used was PolyChord, with both flat and Gaussian priors applied in two different runs. Figures 6.1 and 6.2 show the configuration files used as input in Cobaya for these two runs and figures 6.3 and 6.4 show their respective results.

First, it is important to note the expected appearance of degeneracies. These result in the emergence of multimodalities in the parameter distributions and the presence of multiple dark surfaces in the 2D marginalized posterior plots. In figure 6.3, the appearance of a bimodal structure in the distributions of H and ε is evident, while in the distribution of n_s, there is a hint of a secondary peak, not well resolved from the main one. In the analysis conducted with Gaussian priors, shown in figure 6.4, the situation appears more problematic, as the presence of multiple modes is observed in all distributions. H and ε, in particular, seem to exhibit trimodality, while n_s appears largely degenerate, although it is worth noting the tendency of the distribution to follow a unimodal envelope. A significant issue lies in the partial incompatibility between the distributions resulting from flat priors and those from Gaussian priors. In both cases, however, the expected functional relationship between H and ε, expressed by the relation 3.79, which indicates that they should be proportional, is clearly respected.

I have not been able to identify a definitive reason for the issues in the results of the analysis with Gaussian priors, but I would like to propose two plausible hypotheses: a) Gaussian priors impose stronger constraints on the parameter values than flat priors (unless given unreasonably large variances), as flat priors represent the minimum degree of prior knowledge. This could explain why certain values allowed by the flat-prior results are not equally permitted in the other case, leading to more dispersed corner plots in the latter scenario; b) technical limitations imposed by the available clusters forced a reduction in the precision level required to the program (e.g., low number of live points) to keep execution times within a timeframe compatible with the thesis deadlines (a single execution, even when performed with MPI parallelization across numerous cores, had an average duration of 170 hours). This may have led to insufficient exploration of the parameter space, resulting in incomplete posterior distributions. In any case, the results from both analyses were used as the basis for the subsequent step of the investigation.

6.2 Analysis of Λ

We now study the case under examination within the model presented in this work, specifically an inflationary spectrum given by the expression 3.81 with the amplitude A_s replaced by a function of the parameters

$$A_s = \frac{1}{8\pi^2\varepsilon}\frac{H^2}{M_{\mathrm{Pl}}^2}\Lambda \tag{6.2}$$

Before presenting the result of the analysis, I find it necessary to explain how the results obtained earlier were used to provide some guidance on the priors to be employed in this case. As seen in section 4.5, the expected value for the parameter Λ lies within the range of 10^{-2} Planck masses up to the limiting value M_{Pl}. The value of H during inflation should not depend on the specific inflationary model used, so it is reasonable to assume that the influence of the parameter Λ entirely impacts the value of ε. Consequently, it was decided to use flat priors for this investigation, extended over the intervals where the posterior distributions shown in figure 6.3 are non-zero, appropriately recalibrated to account for the parameter Λ of order $10^{-2}M_{\mathrm{Pl}}$.

It has been observed that the range in which the parameter ε resides extends from 0.0002 to 0.002. Denoting by ε' the value of ε after the inclusion

```
# theory and likelihood input
params:
  H:
    prior:
      min: 1.0e-06
      max: 2.0e-05
    ref:
      dist: norm
      loc: 1.28e-05
      scale: 9.0e-07
    latex: H
  epsi:
    prior:
      min: 0.0001
      max: 0.002
    ref:
      dist: norm
      loc: 0.001
      scale: 0.002
    latex: \epsilon
  ns:
    prior:
      min: 0.8
      max: 1.2
    ref:
      dist: norm
      loc: 0.965
      scale: 0.004
    proposal: 0.001
    latex: n_\mathrm{s}
sampler:
  polychord:
    nlive: 10d
    num_repeats: d
    precision_criterion: 0.1
output: noas
timing: true
```

Figure 6.1: *Cobaya's input for the analysis described in section 6.1 with flat priors.*

```
# theory and likelihood input
params:
  H:
    prior:
      dist: norm
      loc: 1.4e-05
      scale: 4.0e-06
    ref:
      dist: norm
      loc: 1.4e-05
      scale: 1.0e-06
    latex: H
  epsi:
    prior:
      dist: norm
      loc: 0.0012
      scale: 0.0005
    ref:
      dist: norm
      loc: 0.0012
      scale: 0.0002
    latex: \epsilon
  ns:
    prior:
      dist: norm
      loc: 0.965
      scale: 0.009
    ref:
      dist: norm
      loc: 0.965
      scale: 0.004
    proposal: 0.001
    latex: n_\mathrm{s}
sampler:
  polychord:
    nlive: 10d
    num_repeats: d
    precision_criterion: 0.1
output: noas
timing: true
```

Figure 6.2: *Cobaya's input for the analysis described in section 6.1 with Gaussian priors.*

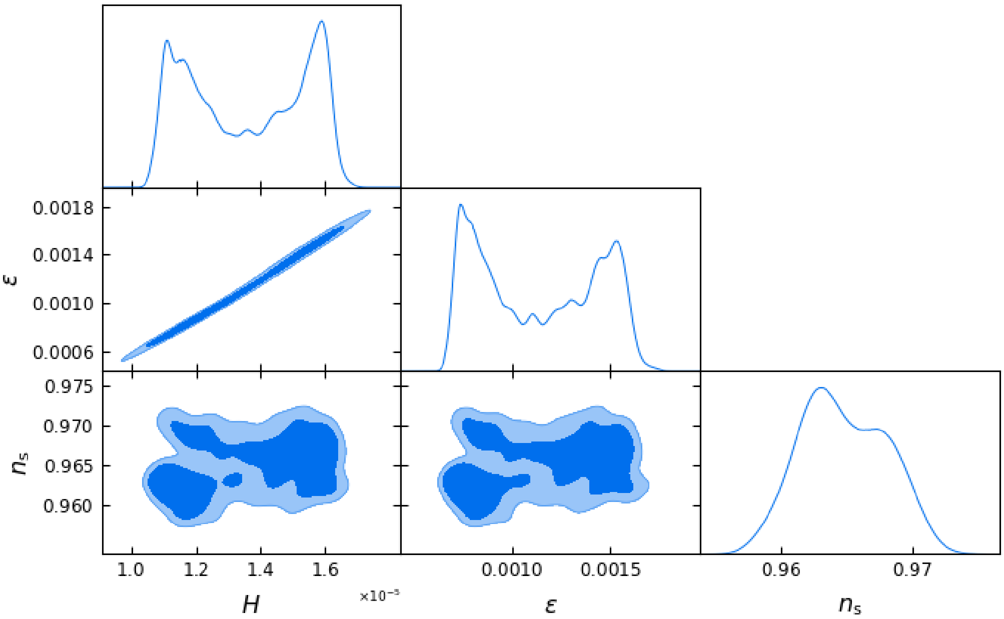

Figure 6.3: *Contour plot of the resulted posteriors for the analysis described in section 6.1 with flat priors.*

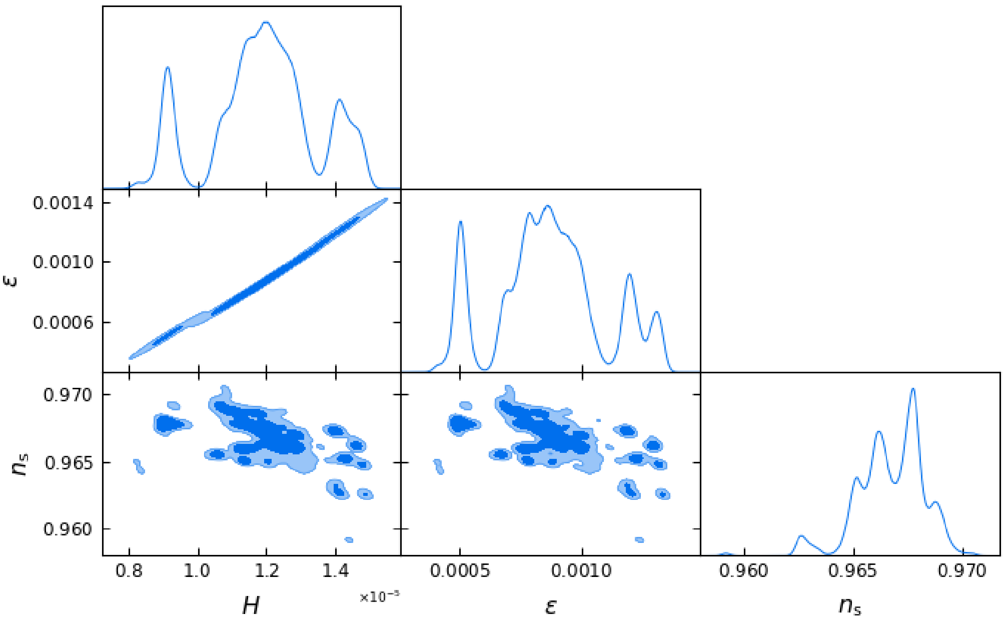

Figure 6.4: *Contour plot of the resulted posteriors for the analysis described in section 6.1 with flat priors.*

of Λ, the following comparison is performed

$$\begin{rcases} A_s = \frac{1}{8\pi^2\varepsilon}\frac{H^2}{M_{\mathrm{Pl}}^2} \\ A_s = \frac{1}{8\pi^2\varepsilon'}\frac{H^2}{M_{\mathrm{Pl}}^2}\Lambda \end{rcases} \Longrightarrow \varepsilon' = \Lambda\varepsilon \tag{6.3}$$

Consequently, the minimum value for ε' occurs for $\varepsilon = 0.0002$, while the maximum value occurs for $\varepsilon = 0.002$. Therefore, the range for the new prior is obtained as

$$\varepsilon' \in \left[2 \times 10^{-6}, 2 \times 10^{-5}\right] \tag{6.4}$$

Taking into account that the introduction of an additional parameter may lead to further degeneracies among all parameters, thereby complicating both the computational process and the interpretative analysis, this study was again conducted using two different approaches. Unlike the preliminary study presented earlier, Gaussian priors were not used this time. Instead, a second execution was performed without sampling the parameter H, assigning it a fixed value. Thus, the role of the parameter H was changed from *sampled* to *fixed*. In the first analysis, however, all parameters were sampled as described in this section. As before, the sampler used was PolyChord.

Figures 6.5 and 6.6 show the configuration files for these two runs. Figure 6.7 shows the result of the analysis of the first run, with all parameters sampled.

As expected, the resulting scenario is challenging to interpret, with most of the contour plots being fragmented, making it difficult to identify regions of higher likelihood. It is reasonable to assume that the computational precision was compromised due to the strong parameter degeneracy, which is why the decision was made to repeat the analysis by fixing the Hubble rate. Before proceeding with observations from the second run, it is worth noting that, unlike the other parameters, the posterior distribution of Λ is very regular and shows a clear bimodality within the anticipated range for this parameter.

Figure 6.8 shows the results of the analysis where the value of H was fixed. For clarity, Figure 6.9 presents the results of the same analysis after removing the first 70% of the sampled points. This was done because, often, the points that best describe the distribution are generated once the program has reached a good level of convergence toward the target distribution. Consequently, it can be helpful to study the shape of the plots generated by the later sampled points. The emerging scenario is surprisingly more regular: the plot for Λ exhibits a clear bimodality, consistent with that seen in Figure 6.7 and with the results of the previous studies [4]; the plot for ε shows a slight bimodality, which remains unresolved even after cleaning, and also suggests that the distribution might extend beyond the initially assumed value range;

the posterior for n_s is actually unimodal; finally, the marginal posteriors are clear and display well-defined contours.

It is crucial to note that the most probable values for the parameter ε differ from those typically used in standard slow-roll inflation models. This is entirely expected and, as hoped when this thesis began and in line with the motivations behind this work, it extends the domain within which different inflation models can be considered plausible, opening up new possibilities for research in this field. Before concluding this thesis, I must specify that many of these analyses were initially conducted using the MCMC sampler, but were not pursued further due to the method's insufficient effectiveness in handling high-dimensional parameter spaces and strong parameter degeneracies.

```
# theory and likelihood input
params
 H:
  prior:
   min: 8.0e-06
   max: 1.5e-05
  ref:
   dist: norm
   loc: 1.0e-05
   scale: 1.0e-06
  latex: H
 epsi:
  prior:
   min: 2.0e-06
   max: 2.0e-05
  ref:
   dist: norm
   loc: 7.0e-06
   scale: 2.0e-06
  latex: \varepsilon
 ns:
  prior:
   dist: norm
   loc: 0.965
   scale: 0.009
  ref:
   dist: norm
   loc: 0.965
   scale: 0.004
  proposal: 0.001
  latex: n_\mathrm{s}
 lamb:
  prior:
   min: 0.001
   max: 0.03
  ref:
   dist: norm
   loc: 0.009
   scale: 0.009
  latex: \Lambda
sampler:
 polychord:
  nlive: 10d
  num_repeats: d
  precision_criterion: 0.1
output: lamb
timing: true
```

Figure 6.5: *Cobaya's input for the analysis described in section 6.2 with all parameters sampled.*

```
# theory and likelihood input
params:
  H: 1.0e-05
  epsi:
    prior:
      min: 2.0e-06
      max: 2.0e-05
    ref:
      dist: norm
      loc: 7.0e-06
      scale: 2.0e-06
    latex: \varepsilon
  ns:
    prior:
      dist: norm
      loc: 0.965
      scale: 0.009
    ref:
      dist: norm
      loc: 0.965
      scale: 0.004
    proposal: 0.001
    latex: n_\mathrm{s}
  lamb:
    prior:
      min: 0.001
      max: 0.03
    ref:
      dist: norm
      loc: 0.009
      scale: 0.009
    latex: \Lambda
sampler:
  polychord:
    nlive: 10d
    num_repeats: d
    precision_criterion: 0.1
output: lamb
timing: true
```

Figure 6.6: *Cobaya's input for the analysis described in section 6.2 with H fixed.*

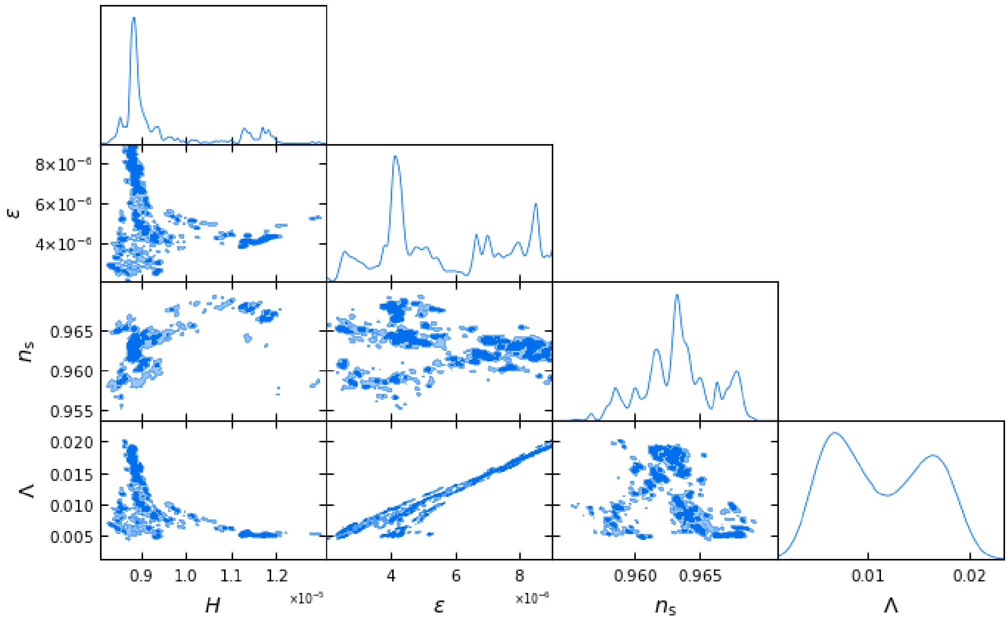

Figure 6.7: *Contour plot of the resulted posteriors for the analysis described in section 6.2 with all parameters sampled.*

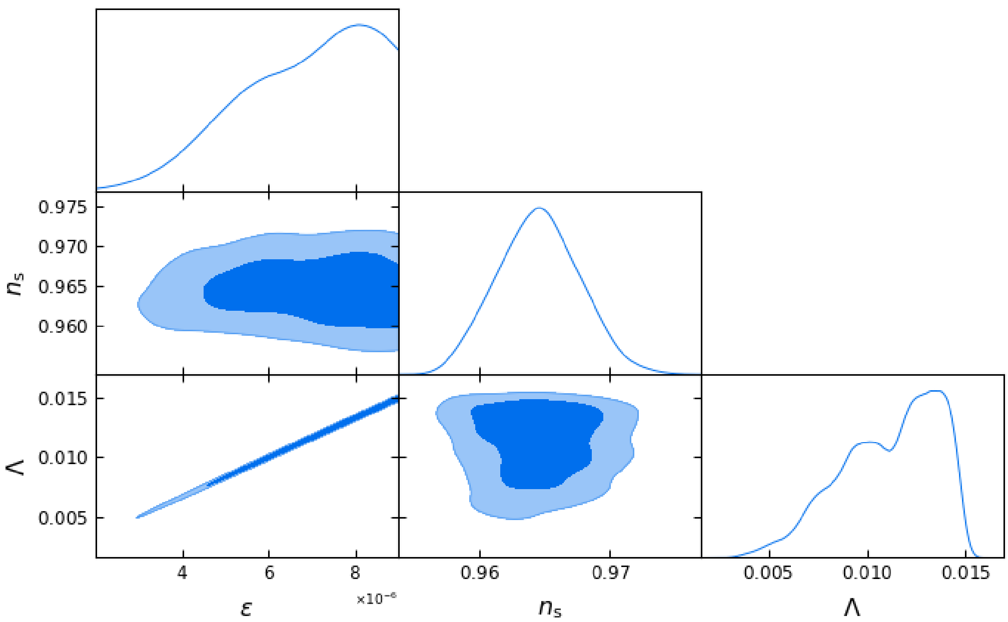

Figure 6.8: *Contour plot of the resulted posteriors for the analysis described in section 6.2 with H fixed.*

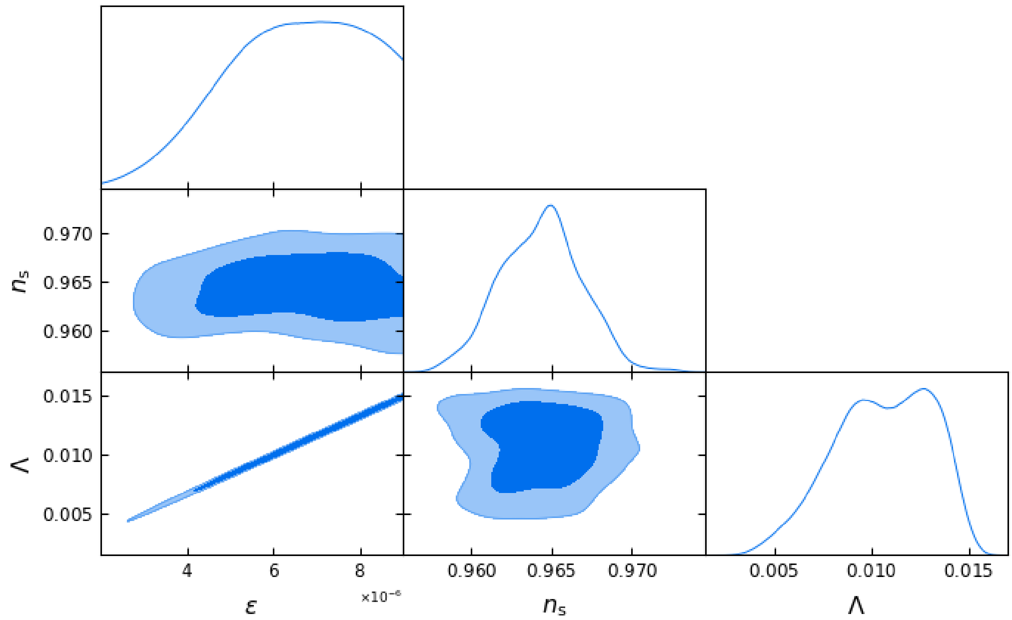

Figure 6.9: *Contour plot of the resulted posteriors for the analysis described in section 6.2 with H fixed, after cleaning.*

CONCLUSIONS

The theoretical framework for describing the formation of CMB anisotropies and large-scale structures is both simple and effective. Its simplicity stems from a distinctive feature of inflation: a quasi de Sitter expansion phase during which the Hubble radius remains nearly constant. Its success is due to the fact that this characteristic naturally leads to a scale-invariant spectrum, consistent with observations. This thesis focuses on the challenge of describing the effects of perturbation dynamics during the primordial stages of inflation, where fluctuations enter a trans-Planckian regime where quantum gravitational effects may become non negligible, and linear approximation may fail. In other words, the study addresses the initial conditions for perturbation modes when they transition to a "classical" regime from the point of view of gravitational interactions. In this context, I considered the model in reference [4], which traces these initial conditions to a preceding stage where perturbations originate from a source term describing interactions with a stochastic background of fluctuations due to gravity effects at very high energies. Specifically, the authors identified this background as the product of Hawking radiation generated by a "Black Hole gas". The outcome of this model is a scale-invariant spectrum with an amplitude dependent on a scale Λ.

Building on this model, the parameter Λ was introduced into the dynamics of the perturbations, and its impact on other inflationary parameters, namely the Hubble parameter and the slow-roll parameter—which describes the characteristics of the inflaton field's potential in the single field slow-roll model—was investigated. A likelihood analysis of the parameter set was performed using advanced computational tools for perturbation dynamics and Bayesian analysis, namely CAMB and Cobaya, with its PolyChord sampler.

The analysis was conducted in successive stages to learn how to manage the appearance of degeneracies in cosmological parameters and to make informed choices for the priors used.

The results of the study show the emergence of degeneracies in all inflationary parameters. The parameter Λ was found to have a value consistent with that estimated by the authors of the model, approximately $\Lambda \simeq 10^{-2} M_{\rm Pl}$. The slow-roll parameter exhibits new degeneracies, providing results that differ from established knowledge regarding inflation.

An interesting continuation of this study could involve incorporating oscillatory features into the Λ-dependent spectrum, as these may arise from inflationary models that consider excited states. The emergence of oscillatory features offers a significant technical advantage, as it mitigates some of the parameter degeneracies and simplifies the computational process.

BIBLIOGRAPHY

[1] N. Aghanim et al. "Planck2018 results: VI. Cosmological parameters". In: *Astronomy &; Astrophysics* 641 (Sept. 2020), A6. ISSN: 1432-0746. DOI: 10.1051/0004-6361/201833910. URL: http://dx.doi.org/10.1051/0004-6361/201833910.

[2] Daniel Baumann. *Cosmology*. Cambridge University Press, 2022.

[3] H. Bouzari Nezhad and F. Shojai. "Effect of α-vacua on the scalar and tensor spectral indices: Slow-roll approximation". In: *Physical Review D* 98.6 (Sept. 2018). ISSN: 2470-0029. DOI: 10.1103/physrevd.98.063512. URL: http://dx.doi.org/10.1103/PhysRevD.98.063512.

[4] Mattia Cielo, Gianpiero Mangano, and Ofelia Pisanti. "Impact of trans-Planckian quantum noise on the primordial gravitational wave spectrum". In: *Physical Review D* 108.4 (Aug. 2023). ISSN: 2470-0029. DOI: 10.1103/physrevd.108.043501. URL: http://dx.doi.org/10.1103/PhysRevD.108.043501.

[5] W. J. Handley, M. P. Hobson, and A. N. Lasenby. "¡scp¿polychord¡/scp¿: nested sampling for cosmology". In: *Monthly Notices of the Royal Astronomical Society: Letters* 450.1 (Apr. 2015), pp. L61–L65. ISSN: 1745-3925. DOI: 10.1093/mnrasl/slv047. URL: http://dx.doi.org/10.1093/mnrasl/slv047.

[6] W. J. Handley, M. P. Hobson, and A. N. Lasenby. "polychord: next-generation nested sampling". In: *Monthly Notices of the Royal Astronomical Society* 453.4 (Sept. 2015), pp. 4385–4399. ISSN: 1365-2966.

DOI: `10.1093/mnras/stv1911`. URL: `http://dx.doi.org/10.1093/mnras/stv1911`.

[7] Antony Lewis. *GetDist: a Python package for analysing Monte Carlo samples*. 2019. arXiv: `1910.13970 [astro-ph.IM]`. URL: `https://arxiv.org/abs/1910.13970`.

[8] Antony Lewis and Sarah Bridle. "Cosmological parameters from CMB and other data: A Monte Carlo approach". In: *Physical Review D* 66.10 (Nov. 2002). ISSN: 1089-4918. DOI: `10.1103/physrevd.66.103511`. URL: `http://dx.doi.org/10.1103/PhysRevD.66.103511`.

[9] Viatcheslav Mukhanov. *Physical Foundations of Cosmology*. Cambridge University Press, 2005.

[10] John Skilling. "Nested sampling for general Bayesian computation". In: *Bayesian Analysis* 1.4 (2006), pp. 833–859. DOI: `10.1214/06-BA127`. URL: `https://doi.org/10.1214/06-BA127`.

[11] Jesús Torrado and Antony Lewis. "Cobaya: code for Bayesian analysis of hierarchical physical models". In: *Journal of Cosmology and Astroparticle Physics* 2021.05 (May 2021), p. 057. ISSN: 1475-7516. DOI: `10.1088/1475-7516/2021/05/057`. URL: `http://dx.doi.org/10.1088/1475-7516/2021/05/057`.

[12] Roberto Trotta. *Bayesian Methods in Cosmology*. 2017. arXiv: `1701.01467 [astro-ph.CO]`. URL: `https://arxiv.org/abs/1701.01467`.

LIST OF FIGURES

1.1 *Illustration of the horizon problem in the conventional cosmologycal model taken from ref. [2]. Past light-cones of two points separated by more than 2° do not overlap.* 8
1.2 *CMB anisotropy as function of multipole moment l, as result of several observations.* 9

2.1 *Plot of the scalar field ϕ as function of N in the quadratic potential scalar field inflation.* 18
2.2 *Plot of the comoving Hubble radius R_H as function of N in the quadratic potential scalar field inflation.* 19
2.3 *Plot of the potential slow-roll parameter ε as function of N in the quadratic potential scalar field inflation.* 19
2.4 *Plot of the Hubble rate as function of N in the quadratic potential scalar field inflation.* 19

3.1 *Quantum fluctuations around the background field ϕ.* 30

4.1 *The obtained power spectrum (here called P^t) normalized to the standard BD spectrum versus the ratio Λ/M_{Pl}. A zoom-in plot is provided for a smaller range of the ratio Λ/M_{Pl}.* 44
4.2 *The degeneracy induced by Λ* 45

5.1 *Converging views in Bayesian inference. Image taken from reference [12]* 49

5.2 *Two different choices for the initial power spectrum produce different CMB spectra after CAMB evaluation. Notice that the oscillatory spectrum determines a lower power at low multipoles.* 56
5.3 *Simplified structure of Cobaya's source, showing classes (squares) and parameters (ellipses).* 57
5.4 *Cobaya's input in YAML format for the use case described in this section. Baseline ΛCDM cosmological parameters definitions (prior, reference pdf, etc.) are omitted here for brevity.* 59
5.5 *1- and 2-d marginalized posteriors for the feature parameters in the use case described in this section.* 60

6.1 *Cobaya's input for the analysis described in section 6.1 with flat priors.* . 64
6.2 *Cobaya's input for the analysis described in section 6.1 with Gaussian priors.* 65
6.3 *Contour plot of the resulted posteriors for the analysis described in section 6.1 with flat priors.* 66
6.4 *Contour plot of the resulted posteriors for the analysis described in section 6.1 with flat priors.* 66
6.5 *Cobaya's input for the analysis described in section 6.2 with all parameters sampled.* 69
6.6 *Cobaya's input for the analysis described in section 6.2 with H fixed.* . . 70
6.7 *Contour plot of the resulted posteriors for the analysis described in section 6.2 with all parameters sampled.* 71
6.8 *Contour plot of the resulted posteriors for the analysis described in section 6.2 with H fixed.* 71
6.9 *Contour plot of the resulted posteriors for the analysis described in section 6.2 with H fixed, after cleaning.* 72